Geochimica et Cosmochimica Acta 348 (2023) 221–238

Contents lists available at ScienceDirect

Geochimica et Cosmochimica Acta

journal homepage: www.elsevier.com/locate/gca

Hydrogeochronology: Resetting the timestamp for subsurface groundwaters

Oliver Warr [a,b,*], Nigel J.T. Smith [c], Barbara Sherwood Lollar [a,d]

[a] Department of Earth Sciences, University of Toronto, Toronto, Ontario M5S 3B1, Canada
[b] Department of Earth and Environmental Sciences, University of Ottawa, Advanced Research Complex, Ottawa, Ontario K1N 6N5, Canada
[c] TRIUMF, Vancouver, BC V6T 2A3, Canada
[d] IPGP, Université Paris Cité, 1 rue Jussieu, 75005 Paris, France

ARTICLE INFO

Article history:
Received 3 October 2022
Accepted 9 March 2023
Available online 16 March 2023
Associate editor: Cécile E. Gautheron

Keywords:
Hydrogeochronology
Radiotracers
Groundwater residence times
14C
Groundwater dating
Subsurface tracer production
Aqueous geochemistry

ABSTRACT

Waters recharging the subsurface contain a variety of naturally occurring geochemical components, the concentrations of which are principally a function of the atmosphere and surface environment. Over time, water-rock interactions and radiogenic processes in the subsurface control a complex geochemical evolution, impacting the initial surface-related signatures associated with recharged groundwaters. The rates of these geochemical changes are considerable in many important geologic settings, requiring characterisation and quantification of the dominant subsurface processes and evolving fluid characteristics. Constraining this is critically important for the discipline of fluid 'age' dating - hydrogeochronology. Age dating, or quantification of fluid residence times is typically evaluated through two categories of tracers; those that are incorporated at the point of recharge and decrease over time through radioactive decay (e.g. ^{3}H, ^{14}C, ^{81}Kr) and those that increase over time (e.g. radiogenic noble gases) due to subsurface production and accumulation in fluids. As these fluids, elements, and tracers have different provenance, the calculated 'age' of any fluid represents the average, or mean residence time, of all components. Likewise, additional mechanisms of subsurface tracer production or loss can have significant bearing on any element-specific calculated residence times. The inevitable temporal discrepancies between tracers can be generated or accentuated in the subsurface which can prove difficult to reconcile in hydrogeochronologic modelling approaches.

By incorporating geochemical data into existing neutron flux-based models, this study evaluates specifically how subsurface production of 'diminishing' tracers in the fluid phase, via neutron capture of parent elements, can produce complexity in the dating of host fluids. The *in situ* rates and production routes of ^{3}H, ^{14}C, ^{36}Cl ^{39}Ar, and ^{81}Kr in different subsurface fluids are modelled for a variety of host rock lithologies to evaluate the effect such baseline crustal production in different geochemical settings may have on calculated residence times within naturally occurring systems. In particular this model provides a quantitative evaluation for how site-specific subsurface radiogeochemistry may result in enhanced baselines of ^{36}Cl, ^{39}Ar, (and potentially ^{14}C) relative to canonical assumptions, and substantially impact residence time estimates calculated from these tracers for a range of subsurface environments. Additionally, we evaluate the role geologic environments can have on low levels of baseline production and calculated residence times for ^{3}H and ^{81}Kr. This study quantitatively evaluates the dependence of geologic environments on these subsurface processes and the impacts this may have on hydrogeochronologic studies. The ability to quantify production of tracers in the subsurface and recalibrate associated residence times in a wide range of geologic settings is of direct relevance to areas such as groundwater resource management, Carbon Capture and Storage, hydrogen storage and nuclear waste management strategies, the hydrocarbon and energy industry, and investigations of the timing and evolution of subsurface microbial life.

1. Introduction and aims

To date, the magnitude and significance of subsurface tracer production as a function of geochemical setting remains poorly

* Corresponding author at: Department of Earth and Environmental Sciences, University of Ottawa, Advanced Research Complex, Ottawa, Ontario K1N 6N5, Canada
E-mail address: owarr@uottawa.ca (O. Warr).

https://doi.org/10.1016/j.gca.2023.03.017
0016-7037/

understood, despite the key role it has in controlling variability and magnitude of tracer production-derived residence times and any relevant 'baselines'. Specifically, few estimates have been placed on production of these tracers within the fluid phase, and the contribution this may have on net subsurface tracer accumulation. This second aspect is particularly critical as accurate constraints on the fluid phase production are required to quantitatively evaluate absolute and relative contributions from the rock phase which, to date, remain poorly constrained (e.g. Andrews et al., 1989; Loosli et al 1989; Andrews et al., 1991; Lehmann and Purtschert, 1997; Yokochi et al., 2012; Johnson et al., 2021; Purtschert et al., 2021; Musy et al., 2022). This study addresses this by investigating the fundamental impact that variations in rock and fluid geochemistry have on subsurface tracer production in the fluid phase for ^{3}H, ^{14}C, ^{36}Cl, ^{39}Ar, and ^{81}Kr, and considers for the first time how this can affect fluid hydrogeochronology and associated migration and mixing models. To achieve this, this study models the combined effect of rock and fluid geochemistry on baseline production of tracers for a range of relevant fluid and rock types. Specifically, it evaluates how site-specific neutron fluxes generated in the host rock can interact with associated fluids to generate these short-lived tracers. Such an estimate not only provides a minimum estimate of this *in situ* baseline but also serves as a future basis to investigate efficacy of rock release in specific environments. Through this approach, better constraints can be placed on addition via tracer production from these subsurface production mechanisms. This will allow greater insight into interpreting fluid provenance and residence times, specifically where complexities arise as highlighted in Fig. 1. Consequently, it will allow for more robust estimates to be placed on fluid origins, volumes, extent and timing of any mixing, as well as improving understanding of subsurface residence times. This study also provides a quantitative evaluation of how susceptible each of these geochronologic tracers may be to *in situ* production as a function specific geologic and geochemical settings. This is important as accurately modelling subsurface hydrology, fluid mechanics and residence times are all central themes in a wide variety of social, academic, industrial, and economic research fields including, but not limited to, groundwater resource management, Carbon Capture and Storage, nuclear waste management strategies, the hydrocarbon and energy industry, and crustal habitability and subsurface biosphere studies (e.g. Ballentine et al., 1991; Lin et al., 2006; Zhou and Ballentine, 2006; Gilfillan et al., 2008; Yokochi et al., 2012; Neretnieks, 2013; Lapworth et al., 2013; Kietäväinen et al., 2014; Tsang et al., 2015; Yizhao et al., 2015; Barry et al., 2016; National Academies of Sciences, Engineering, and Medicine, 2019; Lollar et al., 2019; Danabalan et al., 2022).

1.1. Subsurface tracer production and the formation of in situ baselines

The application of radioisotopes to act as hydrogeological tracers has developed over 60 years. In particular the relatively short-lived isotopes, ^{3}H, ^{14}C, ^{36}Cl as well as recent additional tracers such as ^{39}Ar and ^{81}Kr, have frequently been used to identify the source and age of groundwaters (Schlosser et al., 1988; Clark and Fritz, 1997; Kalin, 2000; Frape et al., 2003; Lippmann et al., 2003; Sturchio et al., 2004; Bethke and Johnson, 2008; Alvarado et al., 2013; Edmunds et al., 2014; Lu et al., 2014; Clark, 2015; Markovich et al., 2021; Purtschert et al., 2021). These isotopes are present in trace level abundance in the atmosphere, and are produced through either anthropogenic activity (e.g., nuclear weapons testing) or naturally through cosmic radiation interacting with atmospheric components. Once produced, these isotopes are incorporated into the subsurface water cycle and can infiltrate geological systems as trace components of recharging groundwater. Over time, these degradative tracers naturally decay into child elements as a function of time since the last atmospheric-groundwater interaction, the rate of which is dependent on the respective radioactive half-lives (Lu et al., 2014; Clark, 2015). Conversely, other tracers, such as the noble gases, accumulate in these fluids over time due to production via naturally occurring subsurface radiogenic reactions (Ballentine and Burnard, 2002; Ozima

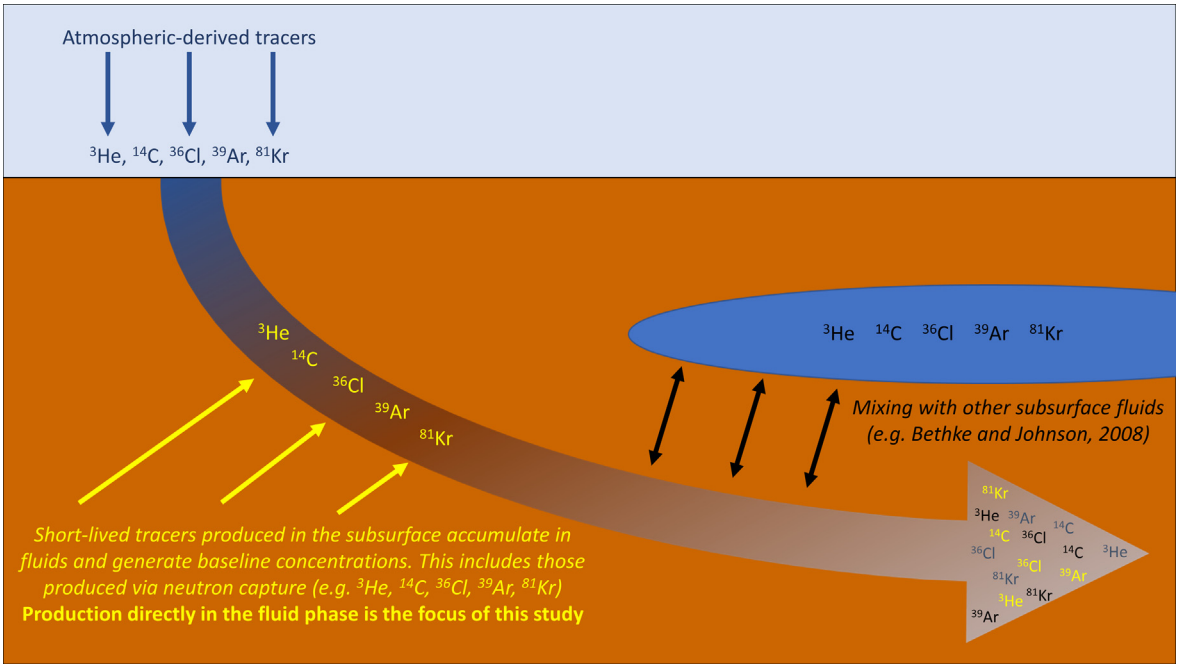

Fig. 1. Schematic highlighting the complexity of short-lived tracers in natural systems. Initially fluids containing atmospheric-derived tracers infiltrate into the subsurface. In the subsurface these tracers decay over time. However, they are also potentially affected by both *in situ* production and mixing and/or exchange with other fluids. The resultant tracer content of the fluids can result in discordant residence times derived from multiple tracers (e.g. Mahara et al., 2001; Onstott et al., 2006a; Lippmann-Pipke et al., 2011; Jasechko et al., 2017; Heard et al., 2018). Production of the tracers directly in the fluid phase is the focus of this study.

and Podosek, 2002). Through precise measuring of the absolute and relative abundances of these degradative or cumulative tracers with respect to initial concentrations and stable isotope counterparts, it is possible to constrain the last time this groundwater was in contact with the atmosphere (Lu et al., 2014; Clark, 2015). This is frequently considered to be the 'age', or residence time, of the water. However, subsurface processes such as fluid migration and/or mixing frequently results in subsurface fluids incorporating multiple components of different provenance as a function of time and/or migration distance (Fig. 1). The consequence of such mixing results in an averaging of both macroscopic and trace content of these fluids based on the concentrations, volumetrics and efficiency of mixing involved. With specific reference to fluid 'ages', these changes can be considered in terms of 'age mass' whereby each fluid volume has an age distribution associated with it. This can be represented by a gaussian curve with the right-hand and left-hand tails representing the oldest and youngest component respectively and has been addressed in previous work by (Goode, 1996; Bethke and Johnson, 2008; Clark, 2015). Consequently, the calculated 'age' from these tracers typically represents the average or mean residence time of all components (Fritz et al., 1989; Goode, 1996; Phillips and Castro, 2003; Bethke and Johnson, 2008; Clark, 2015). Where residence times of one or more of these fluid constituents are sufficiently different, the net effect of fluid interactions can result in noticeably discordant residence times derived from multiple tracers (e.g. Mahara et al., 2001; Onstott et al., 2006a; Lippmann-Pipke et al., 2011; Jasechko et al., 2017; Heard et al., 2018). The complexity introduced by this type of temporal discrepancy between tracers can potentially prove difficult to reconcile in natural systems. Similarly, temporal offsets may also arise between tracer types, even in single component fluids, simply as a function of timescale. Specifically, Warr et al. (2022) recently highlighted how radiogenic/nucleogenic noble gases (^{4}He, ^{21}Ne, ^{40}Ar, ^{136}Xe) may not be efficiently released from host lithologies into associated fluids over geologically short ($\leq$Ma) timescales. As a result, this can potentially create apparent temporal discrepancies between cumulative and degradative tracers. Accordingly, Warr et al. (2022), proposed that within short timescales, short-lived degradative tracers like ^{3}H, ^{14}C, ^{36}Cl, ^{39}Ar, and ^{81}Kr, can be applied to calibrate radiogenic noble gas release models and accurately constrain the shortest timescales over which they are viable. Beyond these two examples, additional complexity may also arise from *in situ* production affecting concentrations and subsurface baselines of these degradative or short-lived tracers (Fig. 1). Although this phenomenon has been noted in previous studies (e.g. Zito et al., 1980; Andrews et al., 1989; Andrews and Fontes, 1992; Lehmann and Purtschert, 1997; Purtschert et al., 2021), this issue of *in situ* production, especially within the fluid phase has, to date, rarely been quantitatively addressed. In particular, despite its potential impact in a wide range of subsurface geochemical settings, the significance of its implications for the broad discipline of hydrogeochronology remains underappreciated. These novel aspects surrounding production in the fluid phase are the primary focus of this work.

The application of degradative tracers to determine groundwater residence times is based on the fundamental general assumption that, starting with a baseline defined by atmospheric conditions at the time of recharge, once isolated from the atmospheric reservoir, these short-lived isotopes become progressively depleted over time due to radioactive decay. Accordingly, the expectation is that older groundwater should have lower abundances of these radioelements. To date, conventional applications of these radioelements typically consider that groundwater infiltrates into geological systems, no secondary process drastically affects these short-lived radioelement baseline concentrations, and all further change is related directly to radioactive decay. Radiocarbon dating approaches address additional processes and elaborate on these assumptions the most systematically. Specifically, for ^{14}C-based fluid geochronology, water rock interactions have the potential to significantly reduce the ^{14}C/^{12}C ratio though ^{14}C matrix diffusion or addition of ^{14}C depleted carbon through processes such as sulfate reduction, carbonate dissolution, or oxidation of ancient organic matter preserved within the host lithology (e.g. Sudicky and Frind, 1981; Maloszewski and Zuber, 1991; Wassenaar et al., 1991; Clark, 2015). It is well recognised, and the established methods integrate such addition of ^{14}C depleted carbon that otherwise result in erroneously elevated residence time estimates (i.e. 'too old') for the fluids unless suitable corrections are applied (e.g. Wigley et al., 1978; Fontes and Garnier, 1979; Clark and Fritz, 1997; Han and Plummer, 2013; Clark, 2015). Typically, however, these are the only processes considered to potentially affect ^{14}C-derived residence times. Frequently overlooked is the potential effect of subsurface production of ^{14}C on calculated mean residence times, as only a few papers from earlier literature have considered this issue (Zito et al., 1980; Barker et al., 1985; Andrews et al., 1989; Lehmann et al., 1993; Bonetti et al., 1997). The general consensus to date has been that any subsurface production of ^{14}C is typically relatively small and therefore does not need to be considered (e.g. Zito et al., 1980; Andrews et al., 1991; Lehmann et al., 1993; Lehmann and Purtschert, 1997; Bethke and Johnson, 2008). Andrews et al. (1989) was one of the few to evaluate this assumption in detail and calculated that for fluids within the Stripa Granite, Sweden, *in situ* natural production of ^{14}C production in the granite host rock could account for an appreciable ($\sim$0.5%) amount of modern carbon which would impact ^{14}C derived residence times (Andrews et al., 1989). The dominant source of this ^{14}C production within the crust was previously determined to be principally through neutron capture by ^{14}N and ^{17}O ($\sim$66 % and $\sim$34% respectively) with minor additions from the ^{13}C, ^{11}B reactions and spontaneous fission of ^{223,224,226}Ra (Zito et al., 1980). However, where uranium contents are significantly elevated in minerals and ores, the ^{11}B alpha particle production route may dominate (e.g. Barker et al., 1985; Jull et al., 1987; Bonetti et al., 1997). In most typical crustal settings, Andrews et al. (1989; 1991) suggested that although ^{14}C is produced in comparable amounts in both the rock matrix and in fracture fluids, only ^{14}C production in the fluids may potentially generate ^{14}C/^{12}C ratios sufficiently above baseline, due to the substantially lower ^{12}C content of fracture fluids. Beyond this early identification of the potential effects for ^{14}C, subsurface production has typically been assumed to be negligible, and the potential range and impact of *in situ* production of ^{14}C on groundwater, and the combined role of, and dependence on, fluid and rock geochemistry remains under-investigated (Zito et al., 1980; Barker et al., 1985; Andrews et al., 1989; Andrews and Fontes, 1992; Lehmann et al., 1993).

A few papers have mentioned similar complexity for the other degradative tracers. For example, although some studies have suggested ^{36}Cl may be reasonably straightforward to model for some settings (e.g. Phillips and Castro, 2003; Sturchio et al., 2004), considerable subsurface production of ^{36}Cl in fluids through neutron capture of ^{35}Cl can generate ^{36}Cl/Cl ratios similar to, or even in excess of initial groundwater ratios within timescales of 1.5 Ma (Fontes et al., 1984; Andrews et al., 1986; Lehmann et al., 1993; Clark and Fritz, 1997; Lippmann et al., 2003; Purtschert et al., 2021). This demonstrates how subsurface production of ^{36}Cl can be both significant and capable of overprinting previous fluid concentrations over relatively short timescales. This tracer instead can provide a minimum groundwater residence time after 5 half-lives (Bentley et al., 1986; Andrews and Fontes, 1992; Clark and Fritz, 1997; Clark, 2015). Likewise, subsurface ^{39}Ar production in host lithologies has also been considered with respect to calibrating ^{40}Ar production and accumulation in the fluid phase (e.g. Yokochi

et al., 2012) as well as more generally in site specific locations (e.g. Loosli et al., 1989; Šrámek et al 2017; Markovich et al., 2021; Purtschert et al., 2021). However, to date, the implications of these limited case studies, and the potential rate and magnitude of multiple tracer production and accumulation in subsurface fluids as a function of geochemical setting has not been considered and evaluated for the discipline as a whole, neither has production directly in the fluid phase been quantified for a wide range of geochemical settings.

With respect to tracer production, neutron capture reactions can produce tracers such as ^{3}H, ^{14}C, ^{36}Cl, ^{39}Ar, and ^{81}Kr, with production occurring both in the host matrix as well as in any associated fluids (e.g. Andrews et al., 1986; Andrews et al., 1989; Florkowski, 1991; Lehmann et al., 1993; Lehmann and Purtschert, 1997; Yokochi et al., 2012; Purtschert et al., 2021). The net accumulation of these tracers in these fluids within a given time through these reactions therefore is the sum of the total *in situ* production in the fluids and the fraction released from the associated lithology, minus the proportion which naturally decays. To date, considerable uncertainty exists regarding the rates of production in both the fluid and in the rock matrix, and the rates and timescales involved with respect to release from rock matrices into associated fluids (Andrews et al., 1989; Andrews et al., 1991; Lehmann and Purtschert, 1997; Purtschert et al., 2021; Musy et al., 2022). Regardless, over sufficient geologic time, production in the host rock and fluids, migration from rock into the fluids, and natural decay of these short-lived tracers will balance out and a steady state, or secular equilibrium concentration is reached. At the same time, any starting (atmospheric-derived) component in the fluid will eventually completely decay. The final baseline concentration, will correspond to a 'baseline residence time' dependent on the geochemistry of the rock and fluids (and affected by tracer release rates into the fluid).

The approach applied here to estimate *in situ* tracer production in groundwater is to evaluate the role of geochemistry on tracer production by combining thermal neutron flux estimates with representative concentrations of the parent elements in the fluid phase. Estimates for parent elements can be made from existing geochemical databases coupled with measured natural isotopic abundances. Constraints on thermal neutron fluxes are less straightforward however. For example, measuring the neutron flux *in situ* involves using highly sensitive counters placed within boreholes for up to 24 h at a time both with the counter exposed and subsequently shielded to the environment in order to quantify the total neutron flux per unit area and the baseline (Andrews et al., 1986). Where boreholes are not present, the counter cannot be fully surrounded by the host rock. In these circumstances alternative shielding setups and additional calculations are used to minimise the complicated influence of large open spaces (Kuhn et al., 1984).

More commonly, various numerical approaches are used to model the subsurface thermal neutron flux by incorporating radioactive decay experiments at a lab or regional scale into calculations involving radioelement and light element abundances in the host rock (Feige et al., 1968; Zito et al., 1980; Kuhn et al., 1984; Andrews et al., 1986; Fabryka-Martin, 1988; Andrews et al., 1989; Lehmann et al., 1993; Šrámek et al., 2017). The approach is not straightforward given the complexity involved in calculating the neutron energy spectra in a rock and quantifying the effect of α particle interaction with all major and trace nuclides in the rock matrix (Kuhn et al., 1984; Andrews et al., 1986; Andrews et al., 1989; Andrews et al., 1991; Lehmann et al., 1993; Šrámek et al., 2017). However, the subsurface geophysics community has well-established approaches within which two key simplifications are typically made: 1. that nuclei of elements present within the host rock are homogenously distributed and 2. that the effect of scaling up elemental concentrations on neutron production is linear with no secondary combinatorial effects observed. The thermal neutron flux is then typically approximated by scaling the radioelement and light element concentrations to specific rock types in experimental laboratory studies (e.g. Feige et al., 1968). On this basis Andrews et al. (1989) calculated a neutron flux in the Stripa Granite of 4.04×10^{-4} cm^{-2} s^{-1}, which was within 15.5% of an independently measured value of 4.7×10^{-4} cm^{-2} s^{-1} (Andrews et al., 1986) using the neutron counter-based approach outlined previously.

This study takes the same approach as Andrews et al. (1989) to estimate neutron fluxes for eight settings. These cover six common lithologies; basalt, sandstone, clay and shales, carbonates, shales, and granites and two additional specific geochemical settings: the well-characterised crystalline basement sites at Kidd Creek Observatory (volcanogenic massive sulfide system) in Timmins, Canada, and the Stripa Granite, 200 km WNW of Stockholm, Sweden (Fig. 2). Kidd Creek was selected for this study as the long-term deep subsurface observatory established there in 2009 (Lollar et al., 2019) has supported multiple studies providing essential context and data. Noble gas studies in particular have demonstrated this fluid-rock system 2.4 km below surface has been isolated for Ma-Ga timescales with negligible biogeochemical inputs from the surface hydrosphere (Sherwood Lollar et al., 2002; Holland et al., 2013; Li et al., 2016; Warr et al., 2018; Lollar et al., 2019; Sherwood Lollar et al., 2021; Warr et al., 2021). Consequently, the highly saline fluids with a high reduced gas content and mafic–ultramafic-felsic and metasedimentary host rock of Kidd Creek represent a natural setting where any short-lived isotope tracer signatures should exclusively be attributable to *in situ* subsurface production. The Stripa Granite system meanwhile represents a dominantly felsic, shallow (~0.4 km), fluid-rock system which has been shown to be more recently affected by meteoric water addition (Moser et al., 1989; Nordstrom et al., 1989) and represents a locality where subsurface production of these tracers has already been considered to some extent (e.g. Andrews et al., 1986; Andrews et al., 1989). For these eight lithologies, three fluid types were considered; modern seawater, Stripa groundwaters, and Kidd Creek fluids. These represent a range of naturally occurring fluids in the subsurface and were selected to demonstrate for the first time how variations in fluid geochemistries in addition to lithologic variations may additionally affect subsurface production of short-lived tracers in a diverse range of crustal settings.

2. Modelling subsurface production of tracers

2.1. Model overview

Building on the methods of Andrews et al. (1989), a model was developed to calculate the subsurface production of ^{3}H, ^{14}C, ^{36}Cl, ^{39}Ar, and ^{81}Kr within subsurface fluids for different lithologies. For subsurface neutron flux for each rock type the approach of Andrews et al. (1989) was used:

$$P_n = {}^{238}N\lambda_{sf}\nu + a[U] + b[Th] \quad (1)$$

where P_n is the production of neutrons per second per gram, ^{238}N is the concentration of ^{238}U atoms per gram, λ_{sf} is the spontaneous fission decay constant for ^{238}U (2.7×10^{-24} per second - De Carvalho et al., 1982), ν is the average number of neutrons per spontaneous fission of ^{238}U (2.2 - Morrison and Pine, 1955), and [U] and [Th] are the concentrations of uranium and thorium in the host rock in ppm. Coefficients a and b relate to the cumulative thermal neutron production due to U and Th-derived alpha particle interactions with light elements in the rock matrix:

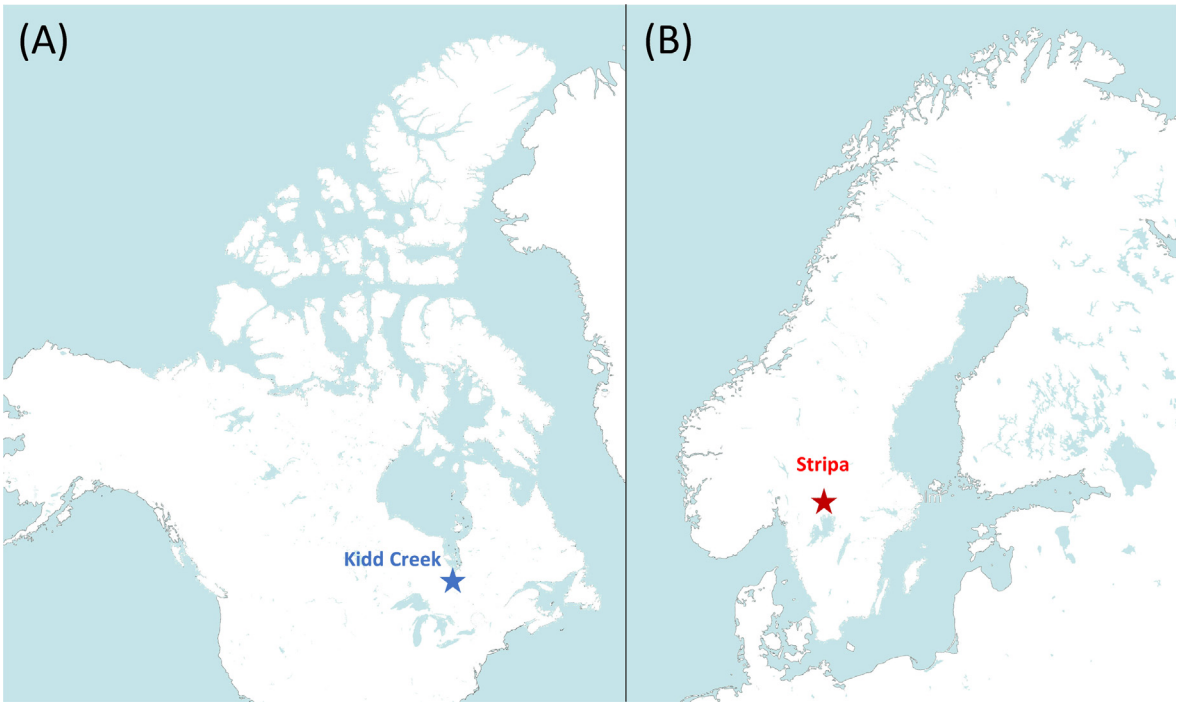

Fig. 2. Location of (A) Kidd Creek in Timmins, Canada (48° 41′ 24″ N, 81° 22′ 0″ W) and (B) Stripa, Sweden (59° 43′ N, 15° 5′ 30″ E). Location maps modified from Vemaps.com. The geochemistries of fluids from these two localities were selected as they represent a spectrum of crystalline basement settings ranging from a highly saline system rich in reduced gases and isolated from surficial processes in a deep crustal VMS setting (Kidd Creek) through to a felsic, low salinity system with (palaeo)meteoric input (Stripa).

$$a = \left(\sum S_i \times F_i \times Y_i^U\right) / \left(\sum S_i \times F_i\right) \quad (2)$$

$$b = \left(\sum S_i \times F_i \times Y_i^{Th}\right) / \left(\sum S_i \times F_i\right) \quad (3)$$

where F_i is the fractional abundance for each element i in the host rock (0–1), S_i represents the mass stopping power of element i at 6.8 MeV, and Y_i^U and Y_i^{Th} are the corresponding neutron yields (Table 2 - Andrews et al., 1989). Neutron production via α particle interaction is considered here for O, F, Na, Mg, Al, Si, K. In this study, representative fractional abundances of these light elements, as well as U, and Th, for basalts, sandstones, clay shales, carbonates, shales and granites are taken from Parker (1967). Where O content of the host rock was not available (shales, sandstones, and carbonates), this was estimated based on standard oxide composition of the dominant elements. For the Stripa Granite, values are taken from Andrews et al. (1989), and for Kidd Creek average values were taken from core samples analysed by Geoscience Laboratories as part of the Ontario Geological Survey, Canada (see Appendix A1. Supplementary Material for details).

To convert the thermal neutron production from Equation (1) into a thermal neutron flux (*nf.*) the following equation was used:

$$nf. = \frac{P_n}{\sigma_m} \quad (4)$$

where σ_m is the weighted-mean absorption cross section for each rock type (Table 3 - Andrews et al., 1989) in cm^2/g. For the Kidd Creek system an average σ_m of 0.0064 was applied to reflect the lithologies at this locality (Table S1). The modelled fluxes are presented in Table 1.

From Table 1, there is good agreement between the modelled fluxes in this work and those previously estimated by Andrews et al. (1989), and all values agree within 0.4% to 29.4% (on average 8.4%). The relatively modest discrepancy observed in calculated neutron flux for carbonates is likely due to the oxygen content for this lithology not being provided in either Parker (1967) or Andrews et al. (1989) and so being estimated here based on standard oxide composition of the dominant elements. The overall good consistency between the modelled neutron fluxes presented here and those from the previous study of Andrews et al., (1989) validates this model's ability to reproduce neutron fluxes in line with the previously published approach for the wide spectrum of potential lithologies considered in this study.

Table 1
Comparison of neutron fluxes calculated for this work compared to those previously published values by Andrews et al. (1989) where available. N/A indicates previous published values were not available. Overall good agreement (<30%) is reached between the calculated fluxes.

Geologic Setting	Calculated neutron flux ($n/cm^2\ s^{-1}$) (This work)	Neutron flux ($n/cm^2\ s^{-1}$) (Andrews et al. 1989)	Difference (%)
Kidd Creek	1.27×10^{-5}	N/A	N/A
Basalt	1.81×10^{-5}	1.60×10^{-5}	13.3%
Sandstone	4.79×10^{-6}	4.60×10^{-6}	4.2%
Clay and shale	3.07×10^{-5}	3.00×10^{-5}	2.3%
Carbonates	2.59×10^{-5}	2.00×10^{-5}	29.4%
Shale	5.19×10^{-5}	N/A	N/A
Granite	6.44×10^{-5}	6.40×10^{-5}	0.6%
Stripa	4.08×10^{-4}	4.07×10^{-4}	0.4%

2.2. Calculating subsurface tracer production in fluids

To calculate the production of each tracer via neutron capture, the abundance of each of the parent isotopes in the host fluid is required. For the three fluids modelled here (seawater, Stripa fluids, and Kidd Creek fracture fluids) the concentrations of each parent isotope are provided in Table 2.

For seawater and the Stripa fluids, elemental concentrations are from the literature. For Kidd Creek fracture fluids, an average fluid

Table 2
Production routes and concentrations of parent isotopes for ^{3}H. ^{14}C, ^{36}Cl, ^{39}Ar, and ^{81}Kr through thermal neutron capture. Production routes and reaction cross sections are from Andrews et al. (1989). Given that ^{39}Ar production can also additionally occur via higher energy neutrons these pathways represent a minimum, or conservative, production of this tracer (see main text). Concentration of parent isotopes are given for each fluid in the last three columns. Elemental concentrations for seawater are from Chan et al (2002), Kabay et al. (2010), Cole (2013), Vinson et al. (2013), Wang et al. (2020), He et al. (2020) and Kipfer et al. (2002) for Li, B, C, Cl, K, Ca, and He-N-Ar-Kr respectively. H and O concentrations were calculated from 1 cm^3 of water. Values for Stripa fluids are from Andrews et al. (1989) where available and from seawater at 10 °C for He and Kr (Kipfer et al., 2002). Concentrations for Kidd Creek fluids were calculated from fluid analyses (See Appendix A2. Supplementary Material). To calculate the isotopic abundances presented here from elemental concentrations, natural abundances were used with the exception of ^{3}He from Kidd Creek which was from Warr et al. (2018).

Tracer	Production route	Reaction cross section (barns)	Seawater (atoms/cm^3)	Stripa Fluids (atoms/cm^3)	Kidd Creek Fracture fluids (atoms/cm^3)
^{3}H	^{2}H (n,γ)	0.00052	7.69×10^{18}	7.56×10^{18}	7.88×10^{18}
	^{6}Li (n,α)	940	1.19×10^{15}	1.19×10^{15}	5.83×10^{15}
	^{10}B(n,2α)	1	6.65×10^{16}	2.66×10^{15}	3.85×10^{16}
	^{3}He(n,p)	5330	1.44×10^{06}	1.44×10^{06}	7.64×10^{10}
^{14}C	^{14}N(n,p)	1.83	5.95×10^{17}	1.33×10^{18}	1.29×10^{20}
	^{13}C (n,γ)	0.00137	1.55×10^{16}	1.37×10^{15}	4.60×10^{18}
	^{17}O(n,α)	0.235	1.27×10^{19}	1.27×10^{19}	1.27×10^{19}
^{36}Cl	^{35}Cl (n,γ)	43.6	2.50×10^{20}	9.01×10^{18}	1.64×10^{21}
	^{39}K(n,α)	0.0043	5.73×10^{18}	3.59×10^{16}	2.09×10^{18}
^{39}Ar	^{38}Ar (n,γ)	0.8	5.10×10^{12}	6.09×10^{12}	5.10×10^{12}
	^{39}K(n,p)	0.016	5.73×10^{18}	3.59×10^{16}	2.09×10^{18}
	^{42}Ca(n,α)	0.016	4.01×10^{16}	1.65×10^{16}	4.95×10^{18}
^{81}Kr	^{80}Kr (n,γ)	16	4.25×10^{10}	4.25×10^{10}	4.25×10^{10}

composition was calculated based on gas and water compositions and flow rates from a combination of previously-published and additional data presented here in this study alongside all analytical methods (see Appendix A2, Supplementary Material). To calculate the isotopic abundances from published elemental concentrations, natural abundances were used, with the exception of ^{3}He from Kidd Creek which was calculated from the helium ratios reported-borehole 12299 in Warr et al. (2018).

The fluid isotopic concentrations for each parent element (atoms per cm^3) were multiplied by the neutron fluxes (neutrons per cm^2 per second) and the reaction cross sectional areas (in cm^2) to calculate tracer production via neutron capture for each production route (in atoms per cm^3 per second):

$$m_i = (nf. \times [i] \times \sigma_i) \quad (5)$$

where m is the modelled tracer from parent element i, $[i]$ is the concentration of parent element i in the fluid (atoms/cm^3), and σ_i is the reaction cross sectional area for i. Values for each of these are provided in Table 2. The annual production of each tracer through individual production routes and their cumulative total (mt_{ot}) are provided in Table 3. The tracer ratios (R_m) used in the following section were calculated from the cumulative totals (m_{tot}) as follows:

$$R_m = \frac{[m_{tot}]}{[m_x]} \quad (6)$$

where m_x represents the stable isotope/element counterpart to the tracer as specified in Table S4.

2.3. Calculating subsurface tracer concentrations and resulting apparent residence times

To calculate the subsurface evolution of tracers for each lithology and fluid type pairing, a stepwise modelling approach was used. In this model timesteps of 10 days (^{3}H), 20 years (^{14}C), 10,000 years (^{36}Cl), 2 years (^{39}Ar) and 500 years (^{81}Kr) were used. These steps represented 4% or less of the associated half-lives and are evaluated in Section 3.2. For each time step the net change in each tracer concentration from the initial values was calculated based on the production rates and total loss through radioactive decay. The initial concentrations of tracers were calculated by multiplying published tracer isotopic ratios (Table S4) by the concentrations of their respective stable elements in the fluids (Table 2). After a minimum of 30 half-lives, the initial tracer isotope concentrations were negligible, and the tracer isotope concentrations become constant, controlled by the balance of *in situ* production and natural decay. Thereafter the system is at secular equilibrium. To derive apparent residence times at secular equilibrium, the tracer concentrations were incorporated into the calculation of Mace et al. (2017):

$$t = (t_{1/2}/ln2) \times ln(R_m/R_0) \quad (7)$$

where t is the apparent residence time, $t_{1/2}$ is the half-life of the element, R_m is the modelled tracer isotope ratio (Equation (6)), and R_0 is the initial tracer isotope ratio in the fluids (Table S4). In this study, the concentrations of the dominant tracers were considered to be constant over time (i.e. no appreciable addition/loss through biogeochemical or water rock interaction). For simplicity and direct comparison, the initial isotope ratio for each tracer (R_0) was considered uniform for each fluid (Table S4), and all tracer results are discussed here in terms of their apparent or actual residence times, their absolute ratios, and/or with respect to percent modern ($R_m/R_0 \times 100$) (e.g. Andrews et al., 1989; Lehmann and Purtschert, 1997; Purtschert et al., 2021), depending on the disciplinary conventions. For each of the 24 lithology-fluid theoretical pairings considered here (Table 3), a tracer ratio at secular equilibrium was calculated after 548 years (200,000 days) (^{3}H), 250,000 years (^{14}C), 10,000,000 years (^{36}Cl), 10,000 years (^{39}Ar), and 10,000,000 years (^{81}Kr), which represent 44, 33, 44, 44, and 37 half-lives respectively. These ratios are provided in Table S5 and with Equation (7) are used to calculate baseline residence times (Table 4) which are exclusively a function of *in situ* geochemistry, and therefore independent of the recharge/initial component. These secular equilibrium values are confirmed in Section 3.2. In the case of ^{39}Ar production it should be pointed out that this model only considers production via thermal neutron capture via the production routes as outlined in Table 2. However, this is a simplification as Šrámek et al. (2017) demonstrated that the ^{39}K (n,p) pathway is highest for neutron energies above the thermal range considered here. Consequently, applying the approach outlined here provides a conservative and proportional estimate of production in either a fluid or a solid rock phase.

2.4. Estimating uncertainty

In order to provide a first-order estimate of total uncertainty in the model, the uncertainty in neutron flux, and uncertainty in elemental concentration in the fluids were integrated. In order to estimate uncertainty in the neutron flux, first the variation between

Table 3
Tracer production in atoms per cm^3 per year of fluid for each rock type for the three fluids modelled in this study. For each fluid the relative production via each neutron capture reaction (Table 2) is provided in italics and the total production in bold. Uncertainty in the total production is 20% (see main text).

Geologic setting	^{3}H Production															^{36}Cl Production		
	Seawater					Stripa fluids					Kidd Creek fluids					Seawater		
	^{2}H	^{6}Li	^{10}B	^{3}He	**Total**	^{2}H	^{6}Li	^{10}B	^{3}He	**Total**	^{2}H	^{6}Li	^{10}B	^{3}He	**Total**	^{35}Cl	^{39}K	**Total**
Kidd	*1.60 × 10^{-6}*	*4.45 × 10^{-4}*	*2.66 × 10^{-5}*	*3.06 × 10^{-12}*	**4.73 × 10^{-4}**	*1.57 × 10^{-6}*	*4.45 × 10^{-4}*	*1.06 × 10^{-6}*	*3.06 × 10^{-12}*	**4.48 × 10^{-4}**	*1.64 × 10^{-6}*	*2.19 × 10^{-3}*	*1.54 × 10^{-5}*	*1.63 × 10^{-7}*	**2.21 × 10^{-3}**	*4.35*	*9.85 × 10^{-6}*	**4.35**
Basalt	*2.29 × 10^{-6}*	*6.37 × 10^{-4}*	*3.80 × 10^{-5}*	*4.38 × 10^{-12}*	**6.77 × 10^{-4}**	*2.25 × 10^{-6}*	*6.37 × 10^{-4}*	*1.52 × 10^{-6}*	*4.38 × 10^{-12}*	**6.41 × 10^{-4}**	*2.34 × 10^{-6}*	*3.13 × 10^{-3}*	*2.20 × 10^{-5}*	*2.33 × 10^{-7}*	**3.16 × 10^{-3}**	*6.23*	*1.41 × 10^{-5}*	**6.23**
Sandstone	*6.04 × 10^{-7}*	*1.68 × 10^{-4}*	*1.00 × 10^{-5}*	*1.16 × 10^{-12}*	**1.79 × 10^{-4}**	*5.94 × 10^{-7}*	*1.68 × 10^{-4}*	*4.02 × 10^{-7}*	*1.16 × 10^{-12}*	**1.69 × 10^{-4}**	*6.19 × 10^{-7}*	*8.28 × 10^{-4}*	*5.82 × 10^{-6}*	*6.15 × 10^{-8}*	**8.35 × 10^{-4}**	*1.65*	*3.72 × 10^{-6}*	**1.65**
Clay + shale	*3.87 × 10^{-6}*	*1.08 × 10^{-3}*	*6.44 × 10^{-5}*	*7.42 × 10^{-12}*	**1.15 × 10^{-3}**	*3.80 × 10^{-6}*	*1.08 × 10^{-3}*	*2.58 × 10^{-6}*	*7.42 × 10^{-12}*	**1.09 × 10^{-3}**	*3.97 × 10^{-6}*	*5.31 × 10^{-3}*	*3.73 × 10^{-5}*	*3.94 × 10^{-7}*	**5.35 × 10^{-3}**	*1.05 × 10^{1}*	*2.39 × 10^{-5}*	**1.05 × 10^{1}**
Carbonates	*3.26 × 10^{-6}*	*9.10 × 10^{-4}*	*5.43 × 10^{-5}*	*6.26 × 10^{-12}*	**9.67 × 10^{-4}**	*3.21 × 10^{-6}*	*9.10 × 10^{-4}*	*2.17 × 10^{-6}*	*6.26 × 10^{-12}*	**9.15 × 10^{-4}**	*3.34 × 10^{-6}*	*4.47 × 10^{-3}*	*3.14 × 10^{-5}*	*3.33 × 10^{-7}*	**4.51 × 10^{-3}**	*8.89*	*2.01 × 10^{-5}*	**8.89**
Shale	*6.54 × 10^{-6}*	*1.82 × 10^{-3}*	*1.09 × 10^{-4}*	*1.25 × 10^{-11}*	**1.94 × 10^{-3}**	*6.43 × 10^{-6}*	*1.82 × 10^{-3}*	*4.35 × 10^{-6}*	*1.25 × 10^{-11}*	**1.83 × 10^{-3}**	*6.70 × 10^{-6}*	*8.97 × 10^{-3}*	*6.30 × 10^{-5}*	*6.67 × 10^{-7}*	**9.04 × 10^{-3}**	*1.78 × 10^{1}*	*4.03 × 10^{-5}*	**1.78 × 10^{1}**
Granite	*8.11 × 10^{-6}*	*2.26 × 10^{-3}*	*1.35 × 10^{-4}*	*1.56 × 10^{-11}*	**2.41 × 10^{-3}**	*7.98 × 10^{-6}*	*2.26 × 10^{-3}*	*5.40 × 10^{-6}*	*1.56 × 10^{-11}*	**2.28 × 10^{-3}**	*8.32 × 10^{-6}*	*1.11 × 10^{-2}*	*7.82 × 10^{-5}*	*8.27 × 10^{-7}*	**1.12 × 10^{-2}**	*2.21 × 10^{1}*	*5.00 × 10^{-5}*	**2.21 × 10^{1}**
Stripa	*5.15 × 10^{-5}*	*1.44 × 10^{-2}*	*8.57 × 10^{-4}*	*9.87 × 10^{-11}*	**1.53 × 10^{-2}**	*5.06 × 10^{-5}*	*1.44 × 10^{-2}*	*3.43 × 10^{-5}*	*9.87 × 10^{-11}*	**1.44 × 10^{-2}**	*5.28 × 10^{-5}*	*7.06 × 10^{-2}*	*4.96 × 10^{-4}*	*5.25 × 10^{-6}*	**7.12 × 10^{-2}**	*1.40 × 10^{2}*	*3.17 × 10^{-4}*	**1.40 × 10^{2}**

Geologic setting	^{36}Cl Production					^{14}C Production												
	Stripa fluids			Kidd Creek fluids		Seawater					Stripa fluids				Kidd Creek fluids			
	^{35}Cl	^{39}K	**Total**	^{35}Cl	^{39}K	**Total**	^{14}N	^{13}C	^{17}O	**Total**	^{14}N	^{13}C	^{17}O	**Total**	^{14}N	^{13}C	^{17}O	**Total**
Kidd	*1.57 × 10^{-1}*	*6.17 × 10^{-8}*	**1.57 × 10^{-1}**	*2.85 × 10^{1}*	*3.59 × 10^{-6}*	**2.85 × 10^{1}**	*4.35 × 10^{-4}*	*8.47 × 10^{-9}*	*1.19 × 10^{-3}*	**1.63 × 10^{-3}**	*9.71 × 10^{-4}*	*7.52 × 10^{-10}*	*1.20 × 10^{-3}*	**2.17 × 10^{-3}**	*9.43 × 10^{-2}*	*2.52 × 10^{-6}*	*1.19 × 10^{-3}*	**9.55 × 10^{-2}**
Basalt	*2.25 × 10^{-1}*	*8.83 × 10^{-8}*	**2.25 × 10^{-1}**	*4.08 × 10^{1}*	*5.13 × 10^{-6}*	**4.08 × 10^{1}**	*6.22 × 10^{-4}*	*1.21 × 10^{-8}*	*1.71 × 10^{-3}*	**2.33 × 10^{-3}**	*1.39 × 10^{-3}*	*1.08 × 10^{-9}*	*1.71 × 10^{-3}*	**3.10 × 10^{-3}**	*1.35 × 10^{-1}*	*3.60 × 10^{-6}*	*1.71 × 10^{-3}*	**1.37 × 10^{-1}**
Sandstone	*5.94 × 10^{-2}*	*2.33 × 10^{-8}*	**5.94 × 10^{-2}**	*1.08 × 10^{1}*	*1.36 × 10^{-6}*	**1.08 × 10^{1}**	*1.64 × 10^{-4}*	*3.20 × 10^{-9}*	*4.51 × 10^{-4}*	**6.15 × 10^{-4}**	*3.67 × 10^{-4}*	*2.84 × 10^{-10}*	*4.52 × 10^{-4}*	**8.19 × 10^{-4}**	*3.57 × 10^{-2}*	*9.52 × 10^{-7}*	*4.51 × 10^{-4}*	**3.61 × 10^{-2}**
Clay + shale	*3.80 × 10^{-1}*	*1.50 × 10^{-7}*	**3.80 × 10^{-1}**	*6.91 × 10^{1}*	*8.69 × 10^{-6}*	**6.91 × 10^{1}**	*1.05 × 10^{-3}*	*2.05 × 10^{-8}*	*2.89 × 10^{-3}*	**3.94 × 10^{-3}**	*2.35 × 10^{-3}*	*1.82 × 10^{-9}*	*2.90 × 10^{-3}*	**5.25 × 10^{-3}**	*2.29 × 10^{-1}*	*6.10 × 10^{-6}*	*2.89 × 10^{-3}*	**2.31 × 10^{-1}**
Carbonates	*3.21 × 10^{-1}*	*1.26 × 10^{-7}*	**3.21 × 10^{-1}**	*5.83 × 10^{1}*	*7.33 × 10^{-6}*	**5.83 × 10^{1}**	*8.88 × 10^{-4}*	*1.73 × 10^{-8}*	*2.44 × 10^{-3}*	**3.32 × 10^{-3}**	*1.98 × 10^{-3}*	*1.54 × 10^{-9}*	*2.44 × 10^{-3}*	**4.43 × 10^{-3}**	*1.93 × 10^{-1}*	*5.14 × 10^{-6}*	*2.44 × 10^{-3}*	**1.95 × 10^{-1}**
Shale	*6.43 × 10^{-1}*	*2.53 × 10^{-7}*	**6.43 × 10^{-1}**	*1.17 × 10^{2}*	*1.47 × 10^{-5}*	**1.17 × 10^{2}**	*1.78 × 10^{-3}*	*3.47 × 10^{-8}*	*4.88 × 10^{-3}*	**6.66 × 10^{-3}**	*3.98 × 10^{-3}*	*3.08 × 10^{-9}*	*4.90 × 10^{-3}*	**8.87 × 10^{-3}**	*3.86 × 10^{-1}*	*1.03 × 10^{-5}*	*4.88 × 10^{-3}*	**3.91 × 10^{-1}**
Granite	*7.98 × 10^{-1}*	*3.14 × 10^{-7}*	**7.98 × 10^{-1}**	*1.45 × 10^{2}*	*1.82 × 10^{-5}*	**1.45 × 10^{2}**	*2.21 × 10^{-3}*	*4.30 × 10^{-8}*	*6.06 × 10^{-3}*	**8.27 × 10^{-3}**	*4.93 × 10^{-3}*	*3.82 × 10^{-9}*	*6.07 × 10^{-3}*	**1.10 × 10^{-2}**	*4.79 × 10^{-1}*	*1.28 × 10^{-5}*	*6.06 × 10^{-3}*	**4.85 × 10^{-1}**
Stripa	*5.06*	*1.99 × 10^{-6}*	**5.06**	*9.19 × 10^{2}*	*1.16 × 10^{-4}*	**9.19 × 10^{2}**	*1.40 × 10^{-2}*	*2.73 × 10^{-7}*	*3.84 × 10^{-2}*	**5.25 × 10^{-2}**	*3.13 × 10^{-2}*	*2.42 × 10^{-8}*	*3.85 × 10^{-2}*	**6.98 × 10^{-2}**	*3.04*	*8.11 × 10^{-5}*	*3.84 × 10^{-2}*	**3.08**

Geologic setting	^{81}Kr Production					^{39}Ar Production												
	Seawater		Stripa fluids		Kidd Creek fluids	Seawater					Stripa fluids				Kidd Creek fluids			
	^{80}Kr	**Total**	^{80}Kr	**Total**	^{80}Kr	**Total**	^{38}Ar	^{39}K	^{42}Ca	**Total**	^{38}Ar	^{39}K	^{42}Ca	**Total**	^{38}Ar	^{39}K	^{42}Ca	**Total**
Kidd	*2.72 × 10^{-10}*	**2.72 × 10^{-10}**	*2.72 × 10^{-10}*	**2.72 × 10^{-10}**	*2.72 × 10^{-10}*	**2.72 × 10^{-10}**	*1.63 × 10^{-9}*	*3.66 × 10^{-5}*	*2.56 × 10^{-7}*	**3.69 × 10^{-5}**	*1.95 × 10^{-9}*	*2.30 × 10^{-7}*	*1.06 × 10^{-7}*	**3.37 × 10^{-7}**	*1.63 × 10^{-9}*	*1.34 × 10^{-5}*	*3.17 × 10^{-5}*	**4.50 × 10^{-5}**
Basalt	*3.89 × 10^{-10}*	**3.89 × 10^{-10}**	*3.89 × 10^{-10}*	**3.89 × 10^{-10}**	*3.89 × 10^{-10}*	**3.89 × 10^{-10}**	*2.33 × 10^{-9}*	*5.24 × 10^{-5}*	*3.66 × 10^{-7}*	**5.28 × 10^{-5}**	*2.78 × 10^{-9}*	*3.29 × 10^{-7}*	*1.51 × 10^{-7}*	**4.83 × 10^{-7}**	*2.33 × 10^{-9}*	*1.91 × 10^{-5}*	*4.53 × 10^{-5}*	**6.44 × 10^{-5}**
Sandstone	*1.03 × 10^{-10}*	**1.03 × 10^{-10}**	*1.03 × 10^{-10}*	**1.03 × 10^{-10}**	*1.03 × 10^{-10}*	**1.03 × 10^{-10}**	*6.16 × 10^{-10}*	*1.39 × 10^{-5}*	*9.68 × 10^{-8}*	**1.40 × 10^{-5}**	*7.36 × 10^{-10}*	*8.68 × 10^{-8}*	*4.00 × 10^{-8}*	**1.28 × 10^{-7}**	*6.16 × 10^{-10}*	*5.05 × 10^{-6}*	*1.20 × 10^{-5}*	**1.70 × 10^{-5}**
Clay + shale	*6.59 × 10^{-10}*	**6.59 × 10^{-10}**	*6.59 × 10^{-10}*	**6.59 × 10^{-10}**	*6.59 × 10^{-10}*	**6.59 × 10^{-10}**	*3.95 × 10^{-9}*	*8.88 × 10^{-5}*	*6.20 × 10^{-7}*	**8.94 × 10^{-5}**	*4.71 × 10^{-9}*	*5.56 × 10^{-7}*	*2.56 × 10^{-7}*	**8.17 × 10^{-7}**	*3.95 × 10^{-9}*	*3.23 × 10^{-5}*	*7.67 × 10^{-5}*	**1.09 × 10^{-4}**
Carbonates	*5.56 × 10^{-10}*	**5.56 × 10^{-10}**	*5.56 × 10^{-10}*	**5.56 × 10^{-10}**	*5.56 × 10^{-10}*	**5.56 × 10^{-10}**	*3.33 × 10^{-9}*	*7.49 × 10^{-5}*	*5.23 × 10^{-7}*	**7.54 × 10^{-5}**	*3.97 × 10^{-9}*	*4.69 × 10^{-7}*	*2.16 × 10^{-7}*	**6.89 × 10^{-7}**	*3.33 × 10^{-9}*	*2.73 × 10^{-5}*	*6.47 × 10^{-5}*	**9.20 × 10^{-5}**
Shale	*1.11 × 10^{-9}*	**1.11 × 10^{-9}**	*1.11 × 10^{-9}*	**1.11 × 10^{-9}**	*1.11 × 10^{-9}*	**1.11 × 10^{-9}**	*6.67 × 10^{-9}*	*1.50 × 10^{-4}*	*1.05 × 10^{-6}*	**1.51 × 10^{-4}**	*7.97 × 10^{-9}*	*9.40 × 10^{-7}*	*4.33 × 10^{-7}*	**1.38 × 10^{-6}**	*6.67 × 10^{-9}*	*5.47 × 10^{-5}*	*1.30 × 10^{-4}*	**1.84 × 10^{-4}**
Granite	*1.38 × 10^{-9}*	**1.38 × 10^{-9}**	*1.38 × 10^{-9}*	**1.38 × 10^{-9}**	*1.38 × 10^{-9}*	**1.38 × 10^{-9}**	*8.28 × 10^{-9}*	*1.86 × 10^{-4}*	*1.30 × 10^{-6}*	**1.87 × 10^{-4}**	*9.88 × 10^{-9}*	*1.17 × 10^{-6}*	*5.37 × 10^{-7}*	**1.71 × 10^{-6}**	*8.28 × 10^{-9}*	*6.78 × 10^{-5}*	*1.61 × 10^{-4}*	**2.29 × 10^{-4}**
Stripa	*8.77 × 10^{-9}*	**8.77 × 10^{-9}**	*8.77 × 10^{-9}*	**8.77 × 10^{-9}**	*8.77 × 10^{-9}*	**8.77 × 10^{-9}**	*5.25 × 10^{-8}*	*1.18 × 10^{-3}*	*8.25 × 10^{-6}*	**1.19 × 10^{-3}**	*6.27 × 10^{-8}*	*7.40 × 10^{-6}*	*3.41 × 10^{-6}*	**1.09 × 10^{-5}**	*5.25 × 10^{-8}*	*4.30 × 10^{-4}*	*1.02 × 10^{-3}*	**1.45 × 10^{-3}**

Table 4
Apparent fluid residence times at secular equilibrium from three starting fluid compositions in eight different lithologies based on subsurface production and natural decay rates using a timestep model (see main text). These apparent residence times were calculated using Equation (7) for each corresponding tracer. The ratios used for these were calculated after 44 (^{3}H), 33 (^{36}Cl), 44 (^{14}C), 44 (^{81}Kr), and 37 (^{39}Ar) half-lives when all tracers within the fluids are the result of *in situ* production and are at a constant concentration (i.e. secular equilibrium), based on *in situ* production and natural decay. These apparent residence times represent the baseline residence time which is dependent on the *in situ* geochemistry and independent of any recharge component. ^{36}Cl values are negative as all modelled ratios at secular equilibrium are greater than the starting ratio (Table S5). These secular equilibrium values are presented graphically in Fig. 3.

Lithology	^{3}H Secular equilibrium residence time (years)			^{36}Cl Secular equilibrium residence time (years)			^{14}C Secular equilibrium residence time (years)			^{81}Kr Secular equilibrium residence time (years)			^{39}Ar Secular equilibrium residence time (years)		
	Seawater	Stripa	Kidd	Seawater	Stripa	Kidd	Seawater	Stripa	Kidd	Seawater	Stripa	Kidd	Seawater	Stripa	Kidd
Kidd	323	323	296	−1,055,780	−1,055,780	−1,055,780	97,028	74,647	110,440	3,263,904	3,263,904	3,263,904	2,377	4,268	2,300
Basalt	316	317	289	−1,211,569	−1,211,568	−1,211,290	94,065	71,684	107,482	3,145,498	3,145,498	3,145,710	2,238	4,129	2,161
Sandstone	340	341	313	−633,049	−633,048	−633,048	105,067	82,686	118,479	3,585,197	3,585,197	3,585,197	2,755	4,646	2,677
Clay + shale	307	308	280	−1,440,493	−1,440,493	−1,440,492	89,712	67,330	103,123	2,971,507	2,971,507	2,971,507	2,034	3,925	1,957
Carbonates	310	311	283	−1,366,365	−1,366,364	−1,366,364	91,121	68,740	104,533	3,027,847	3,027,847	3,027,847	2,100	3,991	2,023
Shale	298	298	271	−1,668,598	−1,668,597	−1,668,597	85,374	62,992	98,785	2,798,138	2,798,138	2,798,138	1,830	3,721	1,753
Granite	294	294	267	−1,762,376	−1,762,375	−1,762,375	83,590	61,209	97,002	2,726,864	2,726,864	2,726,864	1,746	3,637	1,669
Stripa	261	262	234	−2,565,468	−2,565,468	−2,565,468	68,317	45,936	81,729	2,116,481	2,116,481	2,116,481	1,029	2,920	952

the values generated here and those of Andrews (1989) was considered (Table 1) to factor in uncertainty between the neutron fluxes presented here and the previous publication arising from slight differences in the input parameters (e.g. geochemistry) as discussed in Section 2.1. On average, these calculated fluxes agreed within 8.4%. This was then propagated with the noted 15.5% variation between the modelled and measured values at Stripa from Andrews et al. (1986; 1989) to reasonably estimate a first-order total relative neutron flux uncertainty between the model presented here and a natural system following Equation (8):

$$\frac{\Delta nf.}{nf.} = \left[(0.084)^2 + (0.155)^2\right]^{0.5} \tag{8}$$

where Δ represents the uncertainty in the neutron flux and so *Δn.f./n.f.* is the relative uncertainty in the calculated neutron fluxes applied here (17.6%).

With respect to the elemental concentrations, a 5% uncertainty was used based on the typical charge balance error associated with measuring ionic species per the analytical methodology as described in Appendix A2. With production routes and ratios, involving at most four elements (Table 2) this 5% uncertainty was propagated four times to generate a 10% uncertainty associated with the aqueous species considered in Equation (9):

$$\frac{\Delta[i+j+k+l]}{[i+j+k+l]} = \left[(\Delta[i])^2 + (\Delta[j])^2 + (\Delta[k])^2 + (\Delta[l])^2\right]^{0.5} \tag{9}$$

where *i-j* represent the aqueous species and *Δ[i], Δ[j], Δ[j], Δ[l]* are the respective relative uncertainties in the concentration (5%).

Lastly, these two uncertainties derived via Equations (8) and (9) were combined again through standard propagation in Equation (10):

$$m_{tot} = \left[\left(\frac{\Delta nf.}{nf.}\right)^2 + \left(\frac{\Delta[i+j+k+l]}{[i+j+k+l]}\right)^2\right]^{0.5} \tag{10}$$

to generate a total uncertainty of 20%. This 20% uncertainty is considered a reasonable first-order estimate for the concentrations and ratios in the tracer production presented here.

3. Results

3.1. Tracer production

The calculated annual production of each tracer as a function of the eight lithologies and the three starting fluid compositions are provided in Table 3. The 'apparent' residence times derived from the ratios at secular equilibrium (Table S5) are given in Table 4 and plotted in Fig. 3 as a function of neutron flux. These represent the theoretical 'baseline' tracer ages which result exclusively from *in situ* production in the fluids as a function of the aqueous and solid rock geochemistry and are independent of the recharge component in the fluids.

3.2. Validation of modelling approach

Validation of the stepwise approach presented here can be evaluated both in terms of internal model robustness and through comparison to existing data, where available. With respect to robustness and reproducibility, this was confirmed using two approaches. Firstly, the secular equilibrium values calculated here were confirmed by doubling the timescales used to generate the equilibrium values presented Tables 4 and S5. These longer residence times were applied to the seawater in granite geochemical scenario and the resulting tracer ratios were compared to the original ratios (Table S6). This comparison demonstrates that there is

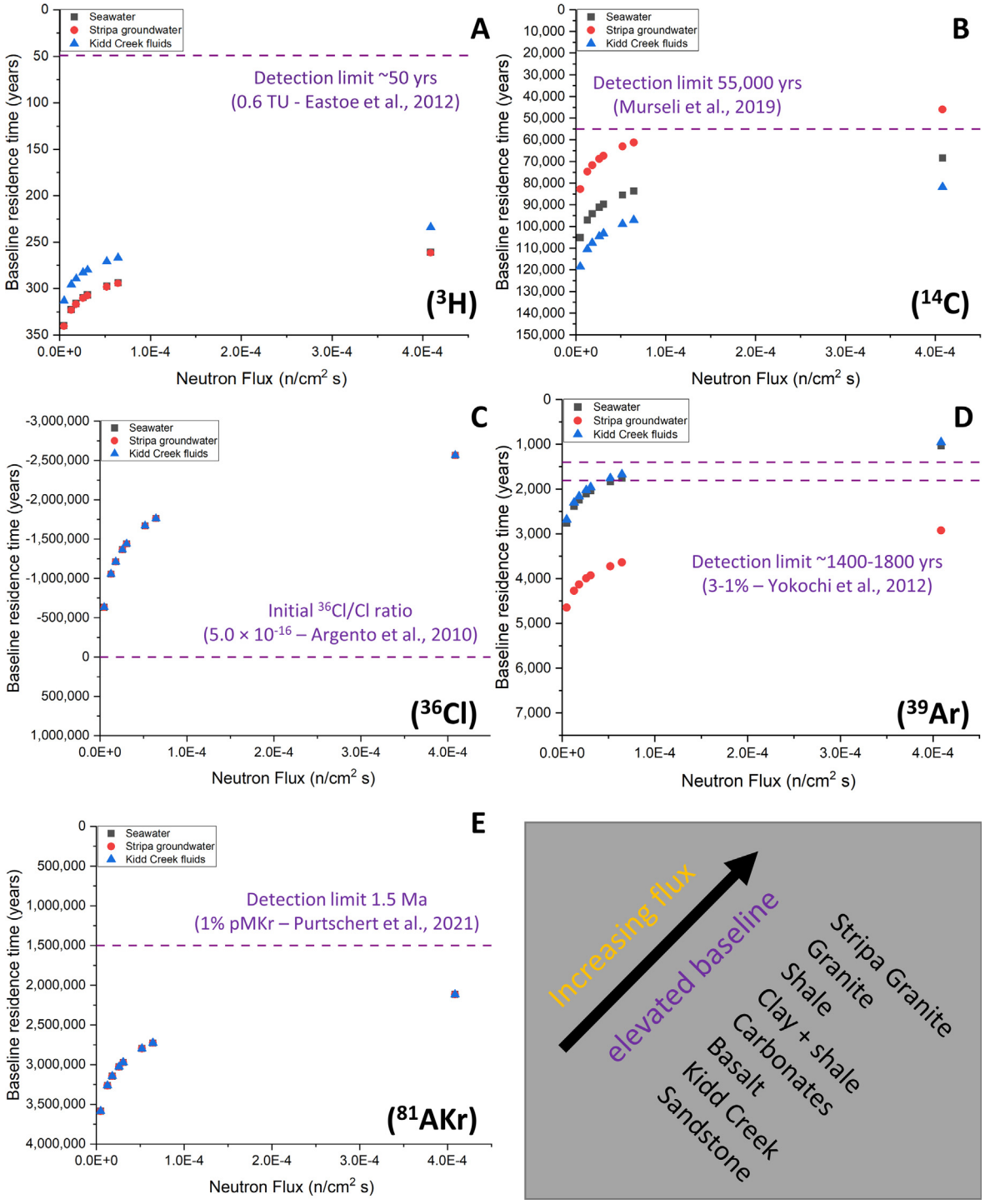

Fig. 3. Apparent fluid residence times for ^{3}H (A), ^{14}C (B), ^{36}Cl (C), ^{39}Ar (D), and ^{81}Kr (E) at secular equilibrium from three starting fluid compositions in eight different lithologies. Plotted data is taken from Table 4 and is based on subsurface production and natural decay rates using a timestep model (see main text). Detection limits from the literature are provided for reference with 'pMKr' and 'TU' representing percentage modern Kr and tritium unit respectively. The relative magnitude of neutron flux as a function of lithology is provided in the inset. This figure demonstrates how both lithology and fluid composition control tracer production in the fluid phase and the resultant baseline apparent residence times.

no change in the tracer ratios by increasing the timescales considered here (37–44 half-lives) by a factor of two. This therefore confirms these values represent secular equilibrium. Secondly, robustness and reproducibility were also evaluated by evaluating a smaller timestep for each tracer to evaluate whether this had any bearing on the calculated values. Specifically, the model timesteps of 10 days (^{3}H), 20 years (^{14}C), 10,000 years (^{36}Cl), 2 years (^{39}Ar) and 500 years (^{81}Kr) were each divided by a factor of 10 to produce alternative timesteps for each tracer which were an order of magnitude smaller than those used in the model. These smaller timesteps were then applied to the seawater in granite geochemical scenario and the tracer ratios generated using these finer timesteps at 44 (^{3}H), 33 (^{36}Cl), 44 (^{14}C), 44 (^{81}Kr), and 37 (^{39}Ar) half-lives were compared with the ratios produced via the original

timesteps. These are provided in Table S7. The data reveals that this order of magnitude increase to the timestep sensitivity results in a negligible (≤1%) change in the tracer ratios at secular equilibrium and highlights the robustness of the model parameters.

With respect to existing data, three lines of evidence support the robustness of the data presented here. Firstly, with respect to the neutron flux, the modelled fluxes are comparable to those previously calculated by Andrews et al. (1989), where that study did so for the same lithologies (Table 1). Additionally, the neutron flux calculated for the Stripa granite both here and by Andrews et al. (1989) agree to within 15% of previous experimental determinations for the Stripa granite (Andrews et al., 1986).

Secondly, in terms of the tracer production, determining the $^{36}Cl/Cl$ secular equilibrium ratio in natural groundwaters has received considerable interest with respect to groundwater dating (e.g. Fontes et al., 1984; Andrews et al., 1986; Phillips et al., 1986; Torgersen et al., 1991; Lippmann et al., 2003). With reference to specific lithologies, the secular equilibrium ratios presented here (Table S5) are comparable to previous estimates by Bentley et al. (1986) for fluids in granites (3.01×10^{14}), sandstones (4.68×10^{15}), shales (1.25×10^{14}), and carbonates (1.09×10^{14}) as well as a ratio specifically calculated by Lehmann et al (1993) for the Stripa granite (1.7×10^{13}). Likewise, these estimates are in good agreement with both ranges modelled for typical crustal settings ($5–30 \times 10^{15}$ - Fontes et al., 1984; Purtschert et al., 2021) and ranges observed in subsurface fluids with residence times of over 1.5 Ma (5 half-lives) ($4–37 \times 10^{15}$ - Lippmann et al., 2003). Consequently, the approach used here generates ^{36}Cl and $^{36}Cl/Cl$ production rates consistent with previous, independent, calculations and empirical observations from natural systems but systematically examines the implications of that knowledge for the first time.

Lastly, the production of ^{14}C modelled here yields $^{14}C/^{12}C$ ratios of 0.4% modern for the Stripa fluids in the Stripa Granite (Table S5). This is consistent with the estimates of Andrews et al. (1989) who indicated that with sufficiently high residence times *in situ* production of ^{14}C could result in a fracture-hosted groundwater with a $^{14}C/^{12}C$ approximately 0.5% of modern ratios. Consequently, the modelled ^{14}C data also is in line with previous modelled results for this specific locality. Once again, examination of the broader implications of this approach for hydrogeochronology has not been carried out until the current study.

Taken together, these three lines of reasoning all highlight how this model is consistent with previous modelling to the extent it has been undertaken, and can generate secular equilibrium ratios comparable to those observed in crustal settings. This, along with the robustness and reproducibility evaluation presented here serves as crucial validation of the model and confirms its ability to generate reasonable estimates of *in situ* production of tracers in the host fluids. This model is applied here to document the effects and impacts for tracer production specifically in the aqueous phase and the corresponding *in situ* baselines for a wide range of geologic and geochemical settings for the first time.

3.3. Subsurface production

As expected, a clear relationship is seen between radioelement concentrations and production for all tracers, with the greatest production associated with lithologies with higher radioelements (Equations (1)–(3)). As a result, the highest secular equilibrium isotope ratios (Table S5) and youngest apparent residence times (Table 4) correspond with radioelement-rich lithologies such as shales and granites. However, the production rates and apparent residence times are not identical between different fluid types and so this approach allows detailed exploration of the controlling role of fluid geochemistry on subsurface tracer production for the first time. This is illustrated here in Fig. 3 and is now evaluated for each tracer.

3.3.1. The production of ^{14}C

Although radioelement content of the host lithology serves as a primary control on production, the geochemistry of the fluids also has an observable effect on subsurface ^{14}C production and $^{14}C/^{12}C$ ratios at secular equilibrium as highlighted in Fig. 3B. The greatest relative *in situ* $^{14}C/^{12}C$ baselines occur where carbon concentrations in the fluids are lowest compared to oxygen and nitrogen, as this combination of parameters results in elevated ^{14}C production in contrast with a lower ^{12}C background. This can be observed in the Stripa fluids where ^{14}N is three orders of magnitude more abundant than ^{13}C and the corresponding baseline residence times for the lithologies investigated range between 83 and 46 ka. Conversely, where carbon concentrations are highest relative to nitrogen and oxygen, the resultant $^{14}C/^{12}C$ at secular equilibrium are lowest and yield the oldest baseline residence times (110 to 82 Ka for Kidd Creek). This is due to the combined effect of a higher ^{12}C baseline which is not offset by the relatively minor ^{14}C production via ^{13}C (n,γ) related to the low reaction cross section. This provides direct quantification of Zito et al. (1980), Andrews and Fontes (1992), and Lehmann et al. (1993) who previously suggested elevated ^{14}C production might occur in instances where C/N ratios are low. These results therefore demonstrate that although baselines are typically low (Table 4) and below detection limits (>55,000 years ^{14}C yr BP - Murseli et al., 2019) the combined role of fluid and rock geochemistry may ultimately still result in appreciable ^{14}C production in fluids where the C/N ratio is low coupled with elevated neutron fluxes. As a consequence, although typically assumed negligible (e.g. Zito et al., 1980; Andrews et al., 1991; Lehmann et al., 1993; Lehmann and Purtschert, 1997; Bethke and Johnson, 2008), the results here demonstrate subsurface production may be significant in some settings and are sensitive to fluid and rock geochemistry. In such cases, ^{14}C-derived fluid residence times younger than 55,000 years (i.e. current detection limits) might erroneously be interpreted as indicative of surface recharge in the absence of other contextual evidence and a critical evaluation of the *in situ* baseline that demonstrate the levels are due to *in situ* production independent of recharge.

3.3.2. The production of ^{36}Cl

In line with previous studies, ^{36}Cl production from ^{35}Cl is demonstrated to be by far the dominant production route (by ~6 orders of magnitude – Table 3). Consequently, the total ^{36}Cl production rate scales proportionally as a function of Cl concentration in the fluids and the $^{36}Cl/Cl$ ratios at secular equilibrium are the same for a given neutron flux as shown in Fig. 3C. Accordingly, although absolute ^{36}Cl production is dependent on the total chlorine content of the fluids, lithology serves as the primary control on the $^{36}Cl/Cl$ and corresponding baseline residence time. In all geochemical scenarios considered here, the modelled $^{36}Cl/Cl$ ratios (Table S5) are substantially above the assumed initial ratio for modern seawater of 5.0×10^{-16}, reported by Argento et al. (2010), resulting in negative apparent residence times. Although the specific apparent residence times are determined by the initial ratio (which is known to vary considerably as a function of geographical location and time e.g. Andrews et al., 1986; Bentley et al., 1986; Lippmann et al., 2003), this study supports the finding that subsurface production of ^{36}Cl can be significant and interfere with models that only consider simple decay over time in line with previous observations as discussed in Section 3.2. Specifically, this considerable *in situ* production has been noted in some locations which have yielded similar $^{36}Cl/Cl$ ratios (Fontes et al., 1984; Andrews et al., 1986; Bentley et al., 1986; Lippmann et al., 2003; Purtschert et al., 2021). This study additionally confirms that these

ratios are principally a function of the host lithology (specifically neutron flux), with fluid composition having a negligible effect, in line with Andrews and Fontes (1992), Lehmann and Purtschert, (1997), Clark (2015) and others.

3.3.3. The production of ^{39}Ar

In all three fluids considered here, ^{39}Ar production is principally via the ^{39}K (n,p) and/or the ^{42}Ca (n,α) production routes, with ^{38}Ar (n,γ) only providing minor contributions (Table 3). Given that ^{42}Ca and ^{39}K use the modelled reaction cross section (Table 2), relative and total production are directly proportional to the abundance of each element (Andrews et al., 1989). With respect to total production, ^{39}Ar production is highest in fluids where the sum total of these aqueous species (^{39}K and ^{42}Ca) is greatest, which in this case is Kidd Creek. In fluids where potassium dominates, such as in seawater and in the Stripa fluid, this serves as the primary production route. However, in deep subsurface fluids (e.g. Kidd Creek) where calcium is more abundant (Frape et al., 2003), ^{39}Ar production should occur principally via this element. The total production of this tracer within the fluid phase alone is shown here to be non-negligible, with baseline or apparent residence times in the fluid phase alone reaching up to 950–2000 years for the more radioelement-rich lithologies (e.g. Stripa) (Fig. 3D). This range overlaps with existing and proposed upper limits of residence times of ~1000–1800 years based on current detection limits (Yokochi et al., 2012; Mace et al., 2017). These results therefore confirm that the baseline subsurface production of ^{39}Ar in the fluid phase may potentially affect residence times for certain geochemical settings. This substantiates the recent hypothesis of Purtschert et al. (2021), who suggested that the ^{39}K (n,p) production route in the fluids may be comparable to production and release from a host lithology.

3.3.4. The production of ^{81}Kr

From Table 2, only ^{80}Kr-based neutron-capture provides a means of producing ^{81}Kr in the host fluids. In this study, seawater, Kidd Creek, and Stripa fluids were all considered to have an initial ^{80}Kr value of seawater at 10 °C (Table 2), consequently all *in situ* production is identical in each fluid and scales purely as a function of neutron flux (Table 3, Fig. 3E). To evaluate alternative starting concentrations, both seawater at 20 °C and freshwater at 4 °C were also modelled and provided in Table S8. As with the case of ^{36}Cl, which also had a single dominant production route, the annual production of ^{81}Kr is greatest in settings where the highest ^{80}Kr and neutron fluxes are observed. This scaling is likewise directly proportional to the total ^{80}Kr concentration and so results in an $^{81}Kr/Kr$ at secular equilibrium which remains exclusively dependent on neutron flux, independent of initial ^{80}Kr concentration. Consequently, the baseline residence times are identical for each fluid in a given rock type and total neutron flux serves as the primary control on the secular equilibrium $^{81}Kr/Kr$ ratio and corresponding baseline residence time.

For the geologic settings modelled here this baseline production gives apparent ages which are 12–16 half-lives and correspond to 0.002 to 0.026% modern, well below the current detection limits (Fig. 3E, Purtschert et al., 2021). Where neutron flux is particularly high, in a radioelement rich environment, as is the case in the Stripa granite, the ^{80}Kr (n,γ) reaction may result in $^{81}Kr/Kr$ ratios as high as 0.165% modern (2.1 Ma residence times) which still does not exceed current detection limits of ~1.5 Ma (1% modern - Purtschert et al., 2021). As a consequence, the results from this model suggest subsurface production through the ^{80}Kr(n,γ) reaction is not liable to meaningfully affect any associated residence time calculations. This is consistent with the study by Purtschert et al. (2021) which similarly concluded ^{81}Kr production via this production route would be negligible in crustal settings. The data in Table 4 therefore continues to support models where a detectable ^{81}Kr concentrations in subsurface fluids are principally associated with atmospheric recharge in most conventional geologic settings with relatively low associated radioelement concentrations (e.g. Sturchio et al., 2004; Yokochi et al., 2019; Purtschert et al., 2021; Kim et al., 2022).

3.3.5. The production of ^{3}H

This model demonstrates production of ^{3}H in the subsurface is relatively insensitive to the geochemical composition of the host fluids. In all fluids the principal production route occurs via the ^{6}Li (n,α) reaction due to the relative abundance of Li and the large cross-sectional area of ^{6}Li for neutron capture (Table 2). Trace production via ^{10}B(n,2α) provides a minor secondary production route of up to 5.6% where the B concentrations are higher in comparison to Li as is the case in seawater. In all cases, despite hydrogen being a major constituent of water, production via ^{2}H(n,γ) is minor (<1%) due to the very low cross-sectional area (Table 2). Although the ^{3}He (n,p) production route is trivial in all cases, for the Kidd Creek fluids, where ^{3}He has accumulated over Ga timescales (Holland et al., 2013; Warr et al., 2018), the increased concentration coupled with the extremely high relative cross-sectional area is capable of producing 4–5 orders of magnitude more ^{3}H than in modern fluids, though still considerably lower than the ^{6}Li (n,α) production route.

In all modelled scenarios, ^{3}H production is very low compared to initial values and, at secular equilibrium, the $^{3}H/^{1}H$ ratio is at least 5 orders of magnitude lower than any starting concentrations, resulting in apparent ages which correspond to 19–28 half lives. This is principally due to a combination of ^{1}H being a major component of the fluids, coupled with the very low production of ^{3}H via ^{2}H(n,γ) (Table 3). These extremely low baseline $^{3}H/^{1}H$ ratios are well below typical detection limits (6×10^{-19} - Eastoe et al., 2012) as shown in Fig. 3A and therefore are not considered to have any meaningful effect on ^{3}H-derived residence times. This serves to highlight and reinforce that any measurable ^{3}H in subsurface fluid samples is highly unlikely to have been produced in the subsurface and instead should have a recent atmospheric source due to recharge (similar to ^{81}Kr). Of all the tracers considered in this paper then, ^{3}H is the least impacted by subsurface production and any associated baseline effects but is included here for completeness.

4. Discussion

4.1. The role of rock and fluid geochemistry in subsurface production

From the results presented here it is clear that variations in both rock type and fluid geochemistry can result in significant changes both in total production and relative production of each tracer within the host fluids via the specified neutron capture production routes. This highlights the key role geochemistry has in tracer production and how it may impact hydrogeochemical models of fluid migration, mixing, and residence times which are used in a wide range of academic and industrial fields.

For the fluid phase geochemistry, this study demonstrates tracer production is highly dependent on parent element concentration. In all cases, absolute production rates for each tracer scale proportionally as a function of parent element concentration in the fluid phase (and neutron flux) as specified in Section 3.3. Of greatest utility is evaluating how relative and net production may affect tracer/stable isotope ratios (e.g. $^{14}C/^{12}C$, $^{36}Cl/Cl$ etc), as this forms the basis of the apparent residence time calculation for the fluids. Where production of a tracer is typically dominated by a single production route involving the element in question (e.g. ^{35}Cl (n,γ) → ^{36}Cl, ^{80}Kr (n,γ) → ^{81}Kr), the fluid geochemistry directly affects the tracer production rate, yet has only minor effect on the

resultant tracer/stable isotope ratio. Consequently, the baseline ratios and corresponding 'residence times' for these tracers are relatively insensitive to fluid geochemistry as demonstrated in Tables S5 and Table 4. For these tracers, the neutron flux coupled with the reaction cross section serves as the principal controls for the secular equilibrium ratios. Conversely, where tracer production occurs through multiple routes, relationships become more complex and fluid chemistry dependent. In instances where tracer production routes are typically dominated by elements unrelated to the tracer/element secular equilibrium ratio, such as is the case for ^{3}H, ^{14}C, and ^{39}Ar, the production rates depend on the concentration of these elements driving production. However, the corresponding secular equilibrium ratios additionally incorporate the abundance of the stable isotope/element the tracer is tied to. Where concentrations of the latter are relatively low, such as is the case of carbon in the Stripa fluids, the corresponding $^{14}C/^{12}C$ secular ratios are amplified compared to fluids where carbon is more abundant (e.g. Kidd Creek fluids). Similarly, for ^{39}Ar, the $^{39}Ar/^{38}Ar$ ratios are highest where the total ^{39}K and ^{42}Ca concentrations are highest in relation to the ^{38}Ar. Such a scenario may naturally occur in situations involving production of ^{39}Ar or ^{81}Kr in a degassed fluid, which can lead to significantly enhanced $^{39}Ar/^{38}Ar$ and $^{81}Kr/Kr$ ratios, as has recently been observed Beatrix Mine (Purtschert et al., 2021). Alternatively, in settings, where the stable element tied to the tracer is considerably more abundant, such as hydrogen where ^{3}H production is concerned, the corresponding (^{3}H/H) is proportionally reduced in all cases.

Lithology acts as primary control on associated neutron flux. This itself has two components associated with it; first and foremost, the radioelement concentration. As Table 1 demonstrates, in lithologies with a higher U, Th concentration (e.g. shales and granites) the associated neutron flux is greater in comparison to low U, Th counterparts (sandstones and mafic–ultramafic rocks). Furthermore, neutron flux is most sensitive to U content. By doubling the U concentration in the models shown here, the neutron flux increases by ~80% in comparison to ~20% when the same is applied to Th. This is due to the net neutron yields being demonstrably higher for the former (Table 5, this work, Table 2 - Andrews et al., 1989) which is a function of the lower production of α particles due to both the longer half-life of ^{232}Th and the lower total production compared to ^{238}U decay. Less frequently considered however, is how the host matrix itself may also act as a secondary control on neutron production and flux. From the data compiled by Andrews et al. (1989), Ballentine and Burnard (2002), and, more recently, Šrámek et al., (2017), there is a considerable difference in neutron yield depending on the target element interacting with the α particles. For example, the reported neutron yield for Na per μg of U is greater compared to that for O by approximately a factor of 50 (Andrews et al., 1989). Consequently, where lithologies have comparable U, Th concentrations but notably different light element concentrations, variations in the overall neutron fluxes may be observable. In the modelling approach outlined here, this geochemical dependence is taken into account with respect to bulk elemental concentrations, although it is noted that mineralogy may result in additional neutron production variability due to crystallographic and grain size considerations (Martel et al., 1990; Ballentine and Burnard, 2002). This additional level of complexity cannot readily be incorporated into this type of modelling and therefore remains an area for future investigation, as similarly highlighted by Šrámek et al. (2017).

Table 5
Coefficients for each lithology to use with Equation (12). Coefficients A and B represent the associated neutron flux per ppm of uranium and thorium respectively for each lithology which scales proportionally as a function of radioelement concentration for a given geochemical composition of the host lithology after Andrews et al (1989).

Geologic setting	A	B
Kidd Creek	7.997×10^{-6}	2.489×10^{-6}
Basalt	7.788×10^{-6}	2.586×10^{-6}
Sandstone	5.545×10^{-6}	1.350×10^{-6}
Clay and shale	4.684×10^{-6}	1.429×10^{-6}
Carbonates	9.885×10^{-6}	2.436×10^{-6}
Shale	6.565×10^{-6}	2.300×10^{-6}
Granite	7.047×10^{-6}	2.206×10^{-6}
Stripa	7.498×10^{-6}	2.356×10^{-6}

4.2. A simplified approach to estimate tracer production

The methodology in this study provides a quantitative assessment of how specific host rock and fluid geochemistry control tracer production. However, this can be considerably simplified to generate a useful, first-order, approximation for each lithology type. To estimate the neutron flux for a given lithology Equation (12) can be applied:

$$nf. = [U]A + [Th]B \quad (12)$$

where *nf.* is the neutron flux (cm^{-2} s^{-1}), [U], [Th] are the concentrations of uranium and thorium in the host rock (ppm), and *A* and *B* are the neutron yields per ppm of uranium and thorium respectively for each lithology (Table 5).

The resultant neutron fluxes can then be multiplied by the concentration of parent elements (atoms/cm^3) and the corresponding reaction cross sections (Table 2) as outlined in Equation (6) to calculate tracer production for each production pathway. These can then be summed to provide a straightforward first order estimate of total production for each tracer for a given geochemical setting. It should be noted though that these production ratios are principally based on the 'average' geochemical compositions of host rocks (Parker, 1967). Differences in the light element content of the specific host rock being modelled and these 'lithology representative' values modelled here will result in deviations from these first order estimates, as discussed in detail in Section 4.1.

4.3. The significance of tracer production and in situ baseline considerations

All tracers are produced *in situ* in the subsurface at some level which ultimately results in an *in situ* baseline level once secular equilibrium is reached. Nonetheless, the significance of these subsurface baseline effects, particularly those focussing on production within the fluid phase, have rarely been addressed for the tracers considered here, in either theory, model or field studies with respect to calculated groundwater residence times. Using the modelling approach outlined here these baseline effects have been evaluated for a combination of lithologies and fluids in subsurface settings. It is clear that geochemistry plays a primary role both in terms of total production and the specific production routes. The significance of these effects however are a function of lithology, fluid geochemistry, and the analytical sensitivity (especially detection limit) for each tracer. Both ^{3}H and ^{81}Kr production are likely produced at relatively low rates with respect to their stable counterpart ^{1}H and ^{80}Kr concentrations, and, as shown here, the corresponding ratios at secular equilibrium and resulting apparent residence times are lower than current detection limits. This study therefore serves to highlight how, under typical crustal conditions. these tracers remain principally tied to baselines set by surficial recharge and conventional assumptions regarding these techniques are largely valid. This is in line with previous studies (e.g. Sturchio et al., 2014; Visser et al., 2014; Lindsey et al., 2019; Yokochi et al., 2019; Purtschert et al., 2021). Conversely, in the case

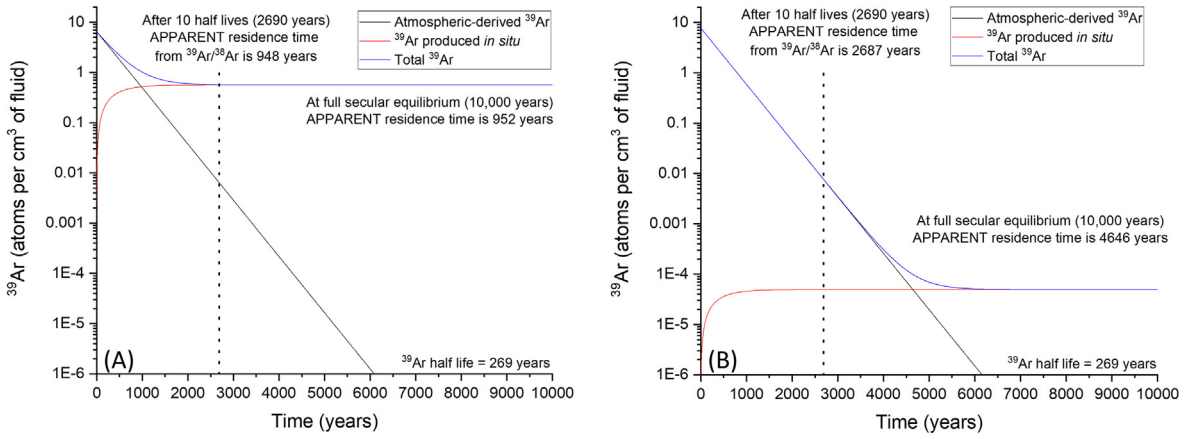

Fig. 4. Temporal evolution of ^{39}Ar concentrations for A) Kidd Creek fluids in Stripa Granite and B) Stripa Fluids in a sandstone. These two configurations represent the maximum and minimum modelled baselines in this study (Table 4). Here the cumulative evolution of the total ^{39}Ar in the system, the ^{39}Ar produced due to subsurface production, and the initial, atmospheric ^{39}Ar, are plotted in blue, red and black lines respectively. Over time the original ^{39}Ar content decreases while the ^{39}Ar produced *in situ* increases until production and decay are balanced and secular equilibrium is reached. At this point the concentration of ^{39}Ar is insensitive to further decay and measured ^{39}Ar no longer reflects residence times but instead represents *in situ* production. In the two examples plotted here this baseline after 10 half-lives (2690 years), shown here by a hatched line, can correspond to between 948 and 2687 years depending on the rock and fluid geochemistries. After 10,000 years (37 half-lives) where subsurface production is the greatest, this apparent residence time slightly increases by 0.4% to 952 years. Where production is the least the apparent residence time increases by 72.9% to 4646 years. The significant difference between the two is due to the rate of production relative to continued decay of the initial atmospheric concentrations. In both cases these "apparent" ages reflect the *in situ* production baseline and would not be representative of groundwater residence times. (For interpretation of the references to colour in this figure legend, the reader is referred to the web version of this article.)

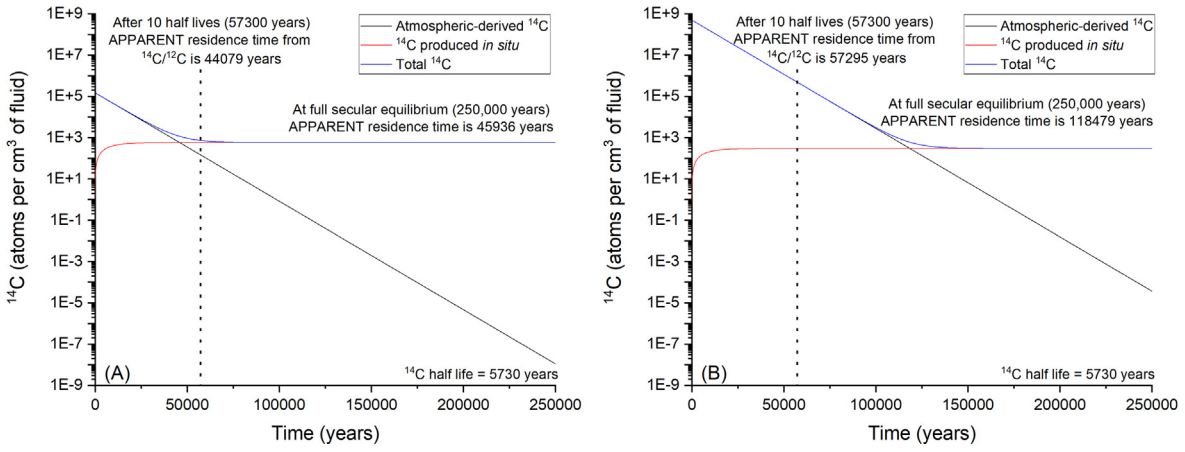

Fig. 5. Evolution of ^{14}C concentrations for A) Stripa fluids in Stripa Granite and B) Kidd Creek fluids in a sandstone. As with ^{39}Ar (Fig. 4) these two configurations represent the maximum and minimum modelled baselines in this study with the total ^{14}C, the subsurface ^{14}C produced, and the initial, atmospheric ^{14}C, plotted in blue, red and black lines respectively. The $^{14}C/^{12}C$ initial ratios are the same (1.176×10^{-12}) but the ^{14}C content of Kidd Creek fluids is higher due to the higher carbon content (Table 2). For this tracer the baseline after 10 half-lives (57,300 years), shown here by a hatched line, can correspond to between 44,079 and 57,295 years depending on the rock and fluid geochemistries being modelled. After 250,000 years (44 half-lives) apparent residence times increase to 45,936 (+4.2%) and 118,479 (+106.8%) years respectively as a function of production and decay in based on the modelled geochemistry and the initial ^{14}C content. (For interpretation of the references to colour in this figure legend, the reader is referred to the web version of this article.)

of ^{36}Cl, subsurface production via neutron capture has a significant and documented effect on secular production rates in all the modelled geochemical environments. This typically results in equilibrium ratios and apparent residence times comparable or even above initial values. This is a finding which is consistent with previous ^{36}Cl-based studies (e.g. Fontes et al., 1984; Andrews et al., 1986; Bentley et al., 1986; Lippmann et al., 2003; Purtschert et al., 2021). In contrast, as demonstrated here, the implications of fluid-based production for the remaining two tracers (^{39}Ar, ^{14}C) are potentially both significant and yet frequently overlooked. The intersection between geochemistry *in situ* production and crucially, the relative importance of these two tracers with respect to their role as dating tools, is addressed further here.

4.4. Challenges for ^{14}C and ^{39}Ar dating of groundwaters

In the case of ^{39}Ar, the stepwise model presented in this study can be further interrogated to evaluate how initial concentrations of ^{39}Ar coupled with the effect of *in situ* production can affect the total ^{39}Ar within a fluid over time. This is given in Fig. 4.

The same can also be applied to ^{14}C as shown in Fig. 5 which shows how ^{14}C production and apparent baselines may evolve over time for A. Stripa type fluids in a Stripa granite setting and B. "Kidd Creek" type saline fluids in a hypothetical sandstone lithology.

From Figs. 4 and 5, the geochemical variations clearly affect whether the secular equilibrium concentrations are significant (e.g. Figs. 4A, 5A), or fall well below standard detection limits

(e.g. Figs. 4B, 5B). Likewise, they both show how the relative baseline production and initial tracer concentrations control the time it takes to reach secular equilibrium. Where initial tracer concentrations are high compared to baseline production, it takes longer for subsurface production to represent the dominant source for each tracer (Figs. 4B, 5B). In real terms, this confirms that, as expected, environments with lower associated ^{14}C and ^{39}Ar production rates will preserve relatively accurate 'apparent' residence times over longer timescales compared to systems where these tracers have enhanced production. The important corollary is that this approach can identify the point beyond which ^{39}Ar or ^{14}C no longer produce data relevant to residence times, but instead reflect the dominance of *in situ* production. Overall, these observations demonstrate how the significance of subsurface production is more complex for these two tracers, in comparison to their ^{36}Cl, ^{3}H, and ^{81}Kr counterparts. Crucially though, it reveals the importance of accurately constraining subsurface geochemistry and the resultant subsurface production when interpreting these tracers. In particular, this study demonstrates how settings with elevated U and Th concentrations (e.g. granites) and/or high $^{14}N/^{12}C$, $(^{42}Ca+^{39}K)/^{38}Ar$ ratios may in particular yield erroneously low (young) ^{14}C and ^{39}Ar fluid residence times. Where U and Th concentrations are particularly high, other tracers such as ^{81}Kr can also be affected. This includes both natural radio-element rich locations (e.g. Oklo, Gabon, and parts of the Witwatersrand Basin - Gauthier-Lafaye et al., 1996; Lippmann et al., 2003; Purtschert et al., 2021) and potentially sites associated with nuclear waste storage, hydrogen storage, or carbon capture. For such geologic storage strategies an inaccurate interpretation of "surface water input" and associated groundwater flow based on what are actually *in situ* elevated baselines can have major implications when evaluating the long-term geologic storage and security (Brydie et al., 2014; Tsang et al., 2015; Zivar et al., 2021).

In addition to careful evaluation of baseline assumptions and models, the findings of this study underscore the importance of understanding tracer production in the fluid phase, especially at sites where a variety of lithologies and mixing of further fluids and/or production and release from the host rock may increase complexity. For example, the application of these tracers can reveal (and potentially quantify) late-stage addition of meteoric water to deeper fluid systems where baselines may have been established for one or more of these tracers. Similarly, they may allow evaluation of potential mixing of subsurface fluids of different provenance (and different tracer content). Alternatively, they can confirm a lack of recent meteoric input and/or mixing and instead confirm residence times sufficiently high enough ($\geq$1.5 Ma) for short lived tracers within the fluid-rock system to attain secular equilibrium, as has already been indicated for ^{36}Cl and, more recently, ^{39}Ar, and ^{81}Kr (e.g. Andrews et al., 1986; Bentley et al., 1986; Lippmann et al., 2003; Clark, 2015; Purtschert et al., 2021). In all cases, integrating geochemical-dependant tracer production adds key constraints to interpreting fluid provenance and residence times, specifically where complexities arise. As a result, additional constraints and more robust estimates can now be placed on fluid volumes, extent and timing of mixing as well as subsurface residence times, by incorporating this aspect into future studies. This aspect will allow detailed evaluation and interrogation of multi-tracer-based approaches, and may provide additional insight into situations where different tracers reveal seemingly conflicting groundwater residence times.

A notable example where tracers showed apparent discordant fluid residence times was highlighted in Heard et al. (2018) where ^{14}C model ages suggested fluids from one sampling location at Masimong Mine, South Africa (MM51940) had residence times of 32 Ka while noble gases indicated much longer residence times of 3.4–10.8 Ma (open system), or 40–97 Ma (closed system). At the time, various mixing and increased noble gas in-growth scenarios were explored and ultimately this $\geq$2 orders of magnitude discrepancy was attributed to contamination due to a modest addition of active ^{14}C through mixing with young waters or air contamination while sampling older groundwaters. However, also mentioned, yet not modelled, was the potential for *in situ* ^{14}C production which may have a higher baseline here given the enhanced U, Th in the region (Lippmann et al., 2003; Silver et al., 2012; Purtschert et al., 2021; Warr et al., 2022). Taking a Stripa fluid composition as a first order estimate for Masimong based on the salinity (2.67 g/L - Onstott et al., 2006a) and the proximity of the measured $\delta^{18}O$ and $\delta^{2}H$ in the fracture fluids to the local meteoric water line (Heard et al., 2018), and considering a sandstone lithology for the Witwatersrand Basin (Nwaila et al., 2017), and using a relevant uranium concentration of up to 100 ppm and a thorium concentration of 5 ppm (Purtschert et al., 2021), the resulting *in situ* production in the fluids could feasibly produce a ^{14}C baseline age of 43,308 years, very close to the value of 32Ka previously published. This analysis resolves the apparent inconsistency noted in the Heard et al. (2018) study. While this straightforward example does not consider additional subsurface processes that may have affected the ^{14}C further (e.g. sulfate reduction, carbonate dissolution) it serves to demonstrate how, although originally discounted, the site-specific geochemistry may control production of a significant proportion of the measured ^{14}C in the fluids. Clearly, in any geologic setting where quantification of the amount and timing of recent surface water recharge are important – from deep geologic waste repositories, to understanding the deep biosphere, the results of this study must be carefully integrated into radiocarbon approaches.

Critically, this study emphasises that although ^{14}C and ^{39}Ar (and ^{36}Cl) remain viable and valuable tracers for groundwater dating (alongside ^{3}H and ^{81}Kr), the *in situ* production of these two tracers in specific geochemical settings may generate appreciable baselines. The findings of this study therefore underscore the need for hydrogeologic models based on these tracers to assess the potential magnitude and impact of such production. Specific applications where this is directly relevant include groundwater resource management where accurately quantifying recharge rates, fluid migration, and residence time is important, especially where subsurface water represents the dominant water supply (Rueedi et al., 2005; Lapworth et al., 2013; Bretzler et al., 2019). Likewise, precise local–regional scale fluid models incorporating fluid residence times, migration and flow are essential for evaluating long-term nuclear waste, carbon capture, or hydrogen storage repositories (Yang et al., 1996; Neretnieks, 2013; Tsang et al., 2015). These represent prime examples where this research may be applied to enhance existing hydrogeologic models.

4.5. Quantifying tracer production and release from host lithology

This study demonstrates how degradative tracer production in the subsurface and variations in both the lithology and host fluids control the absolute and relative production of ^{3}H, ^{14}C, ^{36}Cl, ^{39}Ar, ^{81}Kr in these host fluids, and the corresponding apparent residence times at secular equilibrium. This focus on production in the fluid phase should be incorporated into future studies which otherwise may typically consider tracer production within host lithology followed by migration/release to any associated fluids. To additionally consider production in the host rock follows the same methods as outlined here (with additional incorporation of fission-derived ^{81}Kr), but also requires determining the interaction and release of these tracers into an associated fluid phase, which is significantly more involved (Andrews et al., 1989; Loosli et al 1989; Andrews et al., 1991; Lehmann and Purtschert, 1997; Yokochi et al., 2012; Johnson et al., 2021; Purtschert et al., 2021; Musy

et al., 2022). Specifically, it requires careful consideration of rock-to-water ratios and surface areas, diffusion coefficients within a) crystal lattices, b) grain boundaries and c) microfractures, and localised variability in mineralogy (Lehmann and Purtschert, 1997). Each of these (and the corresponding release factor) are both site and tracer-specific and have previously been identified as the least constrained parameter in these types of study (e.g. Purtschert et al., 2021). One way to evaluate estimates of release has previously been to relate release to groundwater measurements of other tracers, such as ^{222}Rn, which are principally produced in the rock matrix (Andrews et al., 1991; Lehmann and Purtschert, 1997). Although this can provide estimates of surface area, this relationship is also not well constrained and is demonstrably affected by factors such as thermal neutron energy, which controls tracer recoil ranges, and porosity (Andrews et al., 1991). The fluid production approach demonstrated here is a critical first step as it provides a minimum (conservative) concentration of tracers in the fluid phase. As a consequence, this study provides an alternative viable approach to quantitatively determine release coefficients by modelling site-specific tracer baselines for the fluids alone. This can be subtracted from a measured value within the fluids to quantify the tracer component in the fluids derived from the rock itself. The release coefficients as a percentage of the total *in situ* production at secular equilibrium can then be calculated for each tracer corresponding to this additional tracer component. Through this approach the relative inputs from the two *in situ* production sources can be quantified and evaluated, and the combined lithological, mineralogical, and microstructural effects on tracer-derived residence times can be evaluated for a given locality.

This ability to deconvolve the two contributing sources of *in situ* production allows a site-specific assessment of the relative importance of these production routes. This can be demonstrated here using ^{39}Ar production. As shown in this study, production via the ^{39}K (n,p) and/or the ^{42}Ca (n,α) production routes dominate ^{39}Ar production (Table 3). Concentrations of these parent elements in host lithologies are typically in the percent range (Parker, 1967), whereas in modern waters (e.g. seawater) they are both the ppm range (K and Ca ~400 ppm – Wang et al., 2020; He et al., 2020). These elements therefore are approximately two orders of magnitude less than in the rock phase. Considering a porosity of the host rock of <10% adds an additional order of magnitude decrease in the ratios of these elements in the fluid phase relative to the rock phase within a given volume. In this hypothetical scenario then, the contribution from rock phase becomes comparable (or dominates over) *in situ* production directly in the fluid phase when the release coefficient is 0.1% or more of the total production occurring within the rock phase. Critically though, release coefficients are typically poorly constrained and can be highly variable depending on the site-specific settings (e.g. Andrews et al., 1989; Loosli et al 1989; Andrews et al., 1991; Lehmann and Purtschert, 1997; Yokochi et al., 2012; Johnson et al., 2021; Purtschert et al., 2021; Musy et al., 2022). However, as this simplified worked example demonstrates, considering production in the fluid phase as well as in the host lithology provides a means to resolve this uncertainty and accurately evaluate the absolute and relative contributions from both phases simultaneously which is essential for improving existing models of these tracers in the subsurface.

4.6. The effects of tracer partitioning and speciation

The first-order model presented here considers production and accumulation concentration of each tracer in the fluid phase occurs within a single, homogenous geochemical reservoir. While this is applicable to elements such as chlorine, argon, and krypton, which typically exist as simple solutes in solution, this does not consider partitioning of (bio)geochemically more active elements. As demonstrated by the approach needed to initially calculate the net carbon and hydrogen in the case of Kidd Creek fracture fluids, these elements can potentially be distributed between DIC, DOC, hydrocarbons and water (see Appendix A. Supplementary Material). Consequently, although the secular equilibrium ratios of ^{3}H/H and ^{14}C/^{12}C are presented here for the bulk fluids, there may be considerable variation between the distinct molecular reservoirs. These variations will depend on biogeochemical processes which control production and consumption of these molecules, their respective concentrations, and, where applicable, rates of isotope exchange, as has already been demonstrated for ^{14}C (Clark and Fritz, 1997; Slater et al., 2007; Clark, 2015; Simkus et al., 2016). As a result, the bulk secular equilibrium ratios and corresponding baseline residence times for ^{3}H/H and ^{14}C/^{12}C should be considered conservative estimates with the potential for specific molecular reservoirs to concentrate tracers and increase ratios significantly above this 'average' baseline which will depend on both the mechanisms and the rates involved.

5. Conclusions

This study investigates the extent to which degradative tracers (e.g. ^{3}H, ^{14}C, ^{39}Ar, ^{36}Cl, ^{81}Kr) are produced directly in subsurface fluids via neutron interaction for a variety of subsurface settings and emphasises, for the first time, how total tracer production in the fluids, and the corresponding secular equilibrium ratios are both dependent on both rock geochemistry (neutron flux), and fluid geochemistry (parent elements of tracers). While applications of ^{3}H and ^{81}Kr which incorporate conventional assumptions of atmospheric origin and negligible baselines are largely robust, this study highlights how failure to quantitatively evaluate the effects of *in situ* production of ^{36}Cl, ^{39}Ar, ^{14}C can lead to seemingly discordant fluid ages, both between these degradative tracers and with alternative geochronologic approaches, particularly those operating over Ma timescales (e.g. radiogenic noble gases). By incorporating fluid and rock geochemistry, the effects of *in situ* fluid production over time can now be readily factored in, providing higher degrees of accuracy when evaluating fluid provenance, residence times, production and release from the host lithology, and the origin and timing of mixing of subsurface fluid components. This allows a further layer of sophistication to existing models currently being applied to the hydrocarbon and energy industry, Carbon Capture and Storage, hydrogen storage, nuclear waste management, and groundwater resource management, where accurate constraints on hydrogeologic flow and hydrodynamic conditions are essential for evaluating storage potential and security. Lastly, these findings are also applicable to studies focussing on in the deep subsurface where chemolithotrophic processes dominate and habitability is considered to be driven by radiochemical and radiolytic reactions coupled with subsurface hydrology (e.g. Lin et al., 2005; Onstott et al., 2006b; Sherwood Lollar et al., 2014; Magnabosco et al., 2018). In this regard both residence times and production rate calculations of electron donors and acceptors are key components in microbial metabolism driven habitability models and can provide constraints on 'subsurface colonisation' and interpretation of the evolution and sustainability of life in these settings over deep geologic time (Chivian et al., 2008; Lin et al., 2006; Michalski et al., 2018; Sherwood Lollar et al., 2014; Warr et al., 2023; Academies and of Sciences, Engineering, and Medicine, 2019; Academies and of Sciences, Engineering, and Medicine, 2022). The underpinning nucleosynthetic reactions modelled here provide a means to numerically relate the decay of radioelements in the host rock with nucleosynthetic production of elements in the fluids. At the same time, this work allows investigation and quantification of the role aqueous and solid geochemistry can play in the transfer of subsur-

face energy production into a fluid phase. Thus, developing and incorporating the model as proposed here can serve as a basis to provide key constraints on associated radiochemical processes (e.g. radiolysis), such as hydrogen, carbon, sulfur, and nitrogen cycling and their intersection with subsurface habitability models with implications for Earth and beyond (Li et al., 2016, 2021; Sauvage et al., 2021; Sherwood Lollar et al., 2014, 2021; Silver et al., 2012; Tarnas et al., 2021; Warr et al., 2019, 2022, 2023; Academies and of Sciences, Engineering, and Medicine, 2022).

Declaration of Competing Interest

The authors declare that they have no known competing financial interests or personal relationships that could have appeared to influence the work reported in this paper.

Acknowledgements

This study was financially supported by a New Frontiers in Research Fund Exploration grant, the Nuclear Waste Management Organisation, with additional funding provided by the Natural Sciences and Engineering Research Council of Canada Discovery grants. Sherwood Lollar and Smith are a Director and Fellow respectively of the CIFAR Earth 4D Subsurface Science and Exploration program. Thanks are given to H. Tomes for assistance with rock cores.

Appendix A. Supplementary material

The supplementary material for this article includes methods detailing the sampling and analysis of rock and fluid samples. In addition to this, readers will also find additional information dealing the initial ratios of tracers in the fluid and their ratios at secular equilibrium. Lastly, this file also includes a sensitivity analysis and an additional model for ^{81}Kr production based on alternative starting geochemical and physical conditions. All research data presented here are also available as a CSV file. Supplementary material to this article can be found online at https://doi.org/10.1016/j.gca.2023.03.017.

References

National Academies of Sciences, Engineering, and Medicine, 2019. An Astrobiology Strategy for the Search for Life in the Universe. The National Academies Press, Washington, DC.

National Academies of Sciences, Engineering, and Medicine, 2022. Origins, Worlds, and Life: A Decadal Strategy for Planetary Science and Astrobiology 2023-2032. The National Academies Press, Washington, DC.

Alvarado, J.A.C., Paces, T., Purtschert, R., 2013. Dating groundwater in the Bohemian Cretaceous Basin: Understanding tracer variations in the subsurface. Appl. Geochem. 29, 189–198.

Andrews, J.N., Fontes, J.C., Michelot, J.L., Elmore, D., 1986. In-situ neutron flux, ^{36}Cl production and groundwater evolution in crystalline rocks at Stripa, Sweden. Earth Planet. Sci. Lett. 77, 49–58.

Andrews, J.N., Davis, S.N., Fabryka-Martin, J., Fontes, J.C., Lehmann, B.E., Loosli, H.H., Michelot, J.L., Moser, H., Smith, B., Wolf, M., 1989. The in situ production of radioisotopes in rock matrices with particular reference to the Stripa granite. Geochim. Cosmochim. Acta 53, 1803–1815.

Andrews, J.N., Florkowski, T., Lehmann, B.E., Loosli, H.H., 1991. Underground production of radionuclides in the Milk River aquifer, Alberta, Canada. Appl. Geochem. 6, 425–434.

Andrews, J.N., Fontes, J.-C., Iaea, 1992. Importance of the in situ production of ^{36}Cl, ^{36}Ar and ^{14}C in hydrology and hydrogeochemistry. In: Isotope Techniques in Water Resources Development 1991. IAEA, Vienna, pp. 245–269.

Argento, D.C., Stone, J.O., Keith, F.L., Tims, S.G., 2010. Chlorine-36 in seawater. Nucl. Instrum. Methods Phys. Res. Sect. B 268, 1226–1228.

Ballentine, C.J., Burnard, P.G., 2002. Production, release and transport of noble gases in the continental crust. In: Porcelli, D., Ballentine, C.J., Wieler, R. (Eds.), Noble Gases in Geochemistry and Cosmochemistry, Reviews in Mineralogy and Geochemistry Volume 47. first ed. Mineralogical Society of America, Washington DC, pp. 481–538.

Ballentine, C.J., Onions, R.K., Oxburgh, E.R., Horvath, F., Deak, J., 1991. Rare gas constraints on hydrocarbon accumulation, crustal degassing and groundwater flow in the Pannonian Basin. Earth Planet. Sci. Lett. 105, 229–246.

Barker, D., Jull, T.A.J., Donahue, J.D., 1985. Excess carbon-14 abundances in uranium ores: Possible evidence for emission from uranium-series isotopes. Geophys. Res. Lett. 12, 737–740.

Barry, P.H., Lawson, M., Meurer, W.P., Warr, O., Mabry, J.C., Byrne, D.J., Ballentine, C. J., 2016. Noble gases solubility models of hydrocarbon charge mechanism in the Sleipner Vest gas field. Geochim. Cosmochim. Acta 194, 291–309.

Bentley, H.W., Phillips, F.M., Davis, S.N., 1986. Chapter 10 - Chlorine-36 in the terrestrial environment. In: Fritz, P., Fontes, J.Ch. (Eds.), Handbook of Environmental Isotope Geochemistry, Volume 2: The Terrestrial Environment, B. first ed. Elsevier, Amsterdam, pp. 427–480.

Bethke, C.M., Johnson, T.M., 2008. Groundwater age and groundwater age dating. Annu. Rev. Earth Planet. Sci. 36, 121–152.

Bonetti, R., Guglielmetti, A., Poli, G., 1997. The $^{11}B(\alpha, p)$ reaction and its relevance in subsurface ^{14}C production. Appl. Radiat. Isot. 48, 873–876.

Bretzler, A., Stolze, L., Nikiema, J., Lalanne, F., Ghadiri, E., Brennwald, M.S., Rolle, M., Schirmer, M., 2019. Hydrogeochemical and multi-tracer investigations of arsenic-affected aquifers in semi-arid West Africa. Geosci. Front. 10, 1685–1699.

Brydie, J., Jones, D., Jones, J.P., Perkins, E., Rock, L., Taylor, E., 2014. Assessment of baseline groundwater physical and geochemical properties for the quest carbon capture and storage project, Alberta, Canada. Energy Procedia 63, 4010–4018.

Chan, L.H., Starinsky, A., Katz, A., 2002. The behavior of lithium and its isotopes in oilfield brines: Evidence from the Heletz-Kokhav field, Israel. Geochim. Cosmochim. Acta 66, 615–623.

Chivian, D., Brodie, E.L., Alm, E.J., Culley, D.E., Dehal, P.S., DeSantis, T.Z., Gihring, T.M., Lapidus, A., Lin, L.H., Lowry, S.R., Moser, D.P., Richardson, P.M., Southam, G., Wanger, G., Pratt, L.M., Andersen, G.L., Hazen, T.C., Brockman, F.J., Arkin, A.P., Onstott, T.C., 2008. Environmental genomics reveals a single-species ecosystem deep within earth. Science 322, 275–278.

Clark, I., 2015. Groundwater Geochemistry and Isotopes. CRC Press, Boca Raton.

Clark, I.D., Fritz, P., 1997. Environmental Isotopes in Hydrogeology. CRC Press, Boca Raton.

Cole, J.J., 2013. Chapter 6 - The carbon cycle: with a brief introduction to global biogeochemistry. In: Weathers, K.C., Strayer, D.L., Likens, G.E. (Eds.), Fundamentals of Ecosystem Science. first ed. Academic Press, Cambridge, pp. 109–135.

Danabalan, D., Gluyas, J.G., Macpherson, C.G., Abraham-James, T.H., Bluett, J.J., Barry, P.H., Ballentine, C.J., 2022. The principles of helium exploration. Pet. Geosci. 28, petgeo2021-029.

De Carvalho, H.G., Martins, J.B., Medeiros, E.L., Tavares, O.A.P., 1982. Decay constant for the spontaneous-fission process in ^{238}U. Nucl. Instrum. Methods Phys. Res. 197, 417–426.

Eastoe, C.J., Watts, C.J., Ploughe, M., Wright, W.E., 2012. Future Use of Tritium in Mapping Pre-Bomb Groundwater Volumes. Groundwater 50, 87–93.

Edmunds, M., Darling, G., Purtschert, R., Corcho Alvarado, J.A., 2014. Noble gas, CFC and other geochemical evidence for the age and origin of the Bath thermal waters. Appl. Geochem. 40, 155–163.

Fabryka-Martin, J.T., 1988. Production of Radionuclides in the Earth and their Hydrogeologic Significance, with Emphasis on Chlorine-36 and Iodine-129. University of Arizona, Tucson.

Feige, Y., Oltman, B.G., Kastner, J., 1968. Production rates of neutrons in soils due to natural radioactivity. J. Geophys. Res. 73, 3135–3142.

Florkowski, T., 1991. Natural production of radionuclides in geological formations. J. Phys. G: Nucl. Part. Phys. 17, S513.

Fontes, J.C., Brissaud, I., Michelot, J.L., 1984. Hydrological implications of deep production of chlorine-36. Nucl. Instrum. Methods Phys. Res. Sect. B 5, 303–307.

Fontes, J.-C., Garnier, J.-M., 1979. Determination of the initial ^{14}C activity of the total dissolved carbon: A review of the existing models and a new approach. Water Resour. Res. 15, 399–413.

Frape, S.K., Blyth, A.M., Blomqvist, R., McNutt, R.H., Gascoyne, M., 2003. Deep fluids in the continents II Crystaline rocks. In: Holland, H.D., Turekian, K.K. (Eds.), Treatise on Geochemistry. first ed. Pergamon, Oxford, pp. 541–580.

Fritz, P., Fontes, J.C., Frape, S.K., Louvat, D., Michelot, J.L., Balderer, W., 1989. The isotope geochemistry of carbon in groundwater at Stripa. Geochim. Cosmochim. Acta 53, 1765–1775.

Gauthier-Lafaye, F., Holliger, P., Blanc, P.-L., 1996. Natural fission reactors in the Franceville basin, Gabon: A review of the conditions and results of a "critical event" in a geologic system. Geochim. Cosmochim. Acta 60, 4831–4852.

Gilfillan, S.M., Ballentine, C.J., Holland, G., Blagburn, D., Sherwood Lollar, B., Stevens, S., Schoell, M., Cassidy, M., 2008. The noble gas geochemistry of natural CO_2 gas reservoirs from the Colorado Plateau and Rocky Mountain provinces, USA. Geochim. Cosmochim. Acta 72, 1174–1198.

Goode, D.J., 1996. Direct simulation of groundwater age. Water Resour. Res. 32, 289–296.

Han, L.-F., Plummer, L.N., 2013. Revision of Fontes & Garnier's model for the initial ^{14}C content of dissolved inorganic carbon used in groundwater dating. Chem. Geol. 351, 105–114.

He, H., Li, Y., Wang, S., Ma, Q., Pan, Y., 2020. A high precision method for calcium determination in seawater using ion chromatography. Front. Mar. Sci. 7, 231.

Heard, A.W., Warr, O., Borgonie, G., Linage, B., Kuloyo, O., Fellowes, J.W., Magnabosco, C., Lau, M.C.Y., Erasmus, M., Cason, E.D., van Heerden, E., Kieft, T. L., Mabry, J.C., Onstott, T.C., Sherwood Lollar, B., Ballentine, C.J., 2018. South

African crustal fracture fluids preserve paleometeoric water signatures for up to tens of millions of years. Chem. Geol. 493, 379–395.
Holland, G., Sherwood Lollar, B., Li, L., Lacrampe-Couloume, G., Slater, G.F., Ballentine, C.J., 2013. Deep fracture fluids isolated in the crust since the Precambrian era. Nature 497, 357–360.
Jasechko, S., Perrone, D., Befus, K.M., Bayani, Cardenas, M., Ferguson, G., Gleeson, T., Luijendijk, E., McDonnell, J.J., Taylor, R.G., Wada, Y., Kirchner, J.W., 2017. Global aquifers dominated by fossil groundwaters but wells vulnerable to modern contamination. Nat. Geosci. 10, 425–429.
Johnson, C., Lowrey, J.D., Alexander, T., Mace, E., Prinke, A., 2021. Measurements of the emanation of ^{37}Ar and ^{39}Ar from irradiated rocks and powders. J. Radioanal. Nucl. Chem. 329, 969–974.
Jull, A.J.T., Barker, D.L., Donahue, D.J., 1987. On the ^{14}C content in radioactive ores. Chem. Geol. 66, 35–40.
Kabay, N., Güler, E., Bryjak, M., 2010. Boron in seawater and methods for its separation - A review. Desalination 261, 212–217.
Kalin, R.M., 2000. Radiocarbon dating of groundwater systems. In: Cook, P.G., Herczeg, A.L. (Eds.), Environmental Tracers in Subsurface Hydrology. first ed. Springer, US, Boston, pp. 111–144.
Kietäväinen, R., Ahonen, L., Kukkonen, I.T., Niedermann, S., Wiersberg, T., 2014. Noble gas residence times of saline waters within crystalline bedrock, Outokumpu Deep Drill Hole, Finland. Geochim. Cosmochim. Acta 145, 159–174.
Kim, J.H., Ferguson, G., Person, M., Jiang, W., Lu, Z.T., Ritterbusch, F., Yang, G.M., Tyne, R., Bailey, L., Ballentine, C., Reiners, P., McIntosh, J., 2022. Krypton-81 dating constrains timing of deep groundwater flow activation. Geophys. Res. Lett., 49. e2021GL097618.
Kipfer, R., Aeschbach-Hertig, W., Peeters, F., Stute, M., 2002. Noble gases in Lakes and Ground Waters. In: Porcelli, D., Ballentine, C.J., Wieler, R. (Eds.), Noble Gases in Geochemistry and Cosmochemistry, Reviews in Mineralogy and Geochemistry Volume 47. first ed. Mineralogical Society of America, Washington DC, pp. 615–700.
Kuhn, M.W., Davis, S.N., Bentley, H.W., Zito, R., 1984. Measurements of thermal neutrons in the subsurface. Geophys. Res. Lett. 11, 607–610.
Lapworth, D.J., MacDonald, A.M., Tijani, M.N., Darling, W.G., Gooddy, D.C., Bonsor, H. C., Araguás-Araguás, L.J., 2013. Residence times of shallow groundwater in West Africa: Implications for hydrogeology and resilience to future changes in climate. Hydrogeol. J. 21, 673–686.
Lehmann, B.E., Davis, S.N., Fabryka-Martin, J.T., 1993. Atmospheric and subsurface sources of stable and radioactive nuclides used for groundwater dating. Water Resour. Res. 29, 2027–2040.
Lehmann, B.E., Purtschert, R., 1997. Radioisotope dynamics - The origin and fate of nuclides in groundwater. Appl. Geochem. 12, 727–738.
Li, L., Wing, B.A., Bui, T.H., McDermott, J.M., Slater, G.F., Wei, S., Lacrampe-Couloume, G., Sherwood Lollar, B., 2016. Sulfur mass-independent fractionation in subsurface fracture waters indicates a long-standing sulfur cycle in Precambrian rocks. Nat. Commun. 7, 13252.
Li, L., Li, K., Giunta, T., Warr, O., Labidi, J., Sherwood Lollar, B., 2021. N_2 in deep subsurface fracture fluids of the Canadian Shield: Source and possible recycling processes. Chem. Geol. 585, 120571.
Lin, L.H., Hall, J., Lippmann-Pipke, J., Ward, J.A., Sherwood Lollar, B., DeFlaun, M., Rothmel, R., Moser, D., Gihring, T.M., Mislowack, B., Onstott, T.C., 2005. Radiolytic H_2 in continental crust: Nuclear power for deep subsurface microbial communities. Geochem. Geophys. Geosyst. 6, 7.
Lin, L.H., Wang, P.L., Rumble, D., Lippmann-Pipke, J., Boice, E., Pratt, L.M., Sherwood Lollar, B., Brodie, E.L., Hazen, T.C., Andersen, G.L., DeSantis, T.Z., Moser, D.P., Kershaw, D., Onstott, T.C., 2006. Long-term sustainability of a high-energy, low-diversity crustal biome. Science 314, 479–482.
Lindsey, B.D., Jurgens, B.C., Belitz, K., 2019. Tritium as an indicator of modern, mixed, and premodern groundwater age. USGS Scientific Investigations Report 2019-5090. US Geological Survey, Virginia.
Lippmann, J., Stute, M., Torgersen, T., Moser, D.P., Hall, J.A., Lin, L., Borcsik, M., Bellamy, R.E.S., Onstott, T.C., 2003. Dating ultra-deep mine waters with noble gases and ^{36}Cl, Witwatersrand Basin, South Africa. Geochim. Cosmochim. Acta 67, 4597–4619.
Lippmann-Pipke, J., Sherwood Lollar, B., Niedermann, S., Stroncik, N.A., Naumann, R., van Heerden, E., Onstott, T.C., 2011. Neon identifies two billion year old fluid component in Kaapvaal Craton. Chem. Geol. 283, 287–296.
Lollar, G.S., Warr, O., Telling, J., Osburn, M.R., Sherwood Lollar, B., 2019. 'Follow the Water': Hydrogeochemical Constraints on Microbial Investigations 2.4 km Below Surface at the Kidd Creek Deep Fluid and Deep Life Observatory. Geomicrobiol. J. 36, 859–872.
Loosli, H.H., Lehmann, B.E., Balderer, W., 1989. Argon-39, argon-37 and krypton-85 isotopes in Stripa groundwaters. Geochim. Cosmochim. Acta 53, 1825–1829.
Lu, Z.T., Schlosser, P., Smethie, W.M., Sturchio, N.C., Fischer, T.P., Kennedy, B.M., Purtschert, R., Severinghaus, J.P., Solomon, D.K., Tanhua, T., Yokochi, R., 2014. Tracer applications of noble gas radionuclides in the geosciences. Earth Sci. Rev. 138, 196–214.
Mace, E., Aalseth, C., Brandenberger, J., Day, A., Hoppe, E., Humble, P., Keillor, M., Kulongoski, J., Overman, C., Panisko, M., Seifert, A., White, S., Wilcox Freeburg, E., Williams, R., 2017. Methods for using argon-39 to age-date groundwater using ultra-low-background proportional counting. Appl. Radiat. Isot. 126, 9–12.
Magnabosco, C., Lin, L.H., Dong, H., Bomberg, M., Ghiorse, W., Stan-Lotter, H., Pedersen, K., Kieft, T.L., van Heerden, E., Onstott, T.C., 2018. The biomass and biodiversity of the continental subsurface. Nat. Geosci. 11, 707–717.
Mahara, Y., Igarashi, T., Hasegawa, T., Miyakawa, K., Tanaka, Y., Kiho, K., 2001. Dynamic changes in hydrogeochemical conditions caused by tunnel excavation at the Aspo Hard Rock Laboratory (HRL), Sweden. Appl. Geochem. 16, 291–315.
Maloszewski, P., Zuber, A., 1991. Influence of Matrix Diffusion and Exchange Reactions on Radiocarbon Ages in Fissured Carbonate Aquifers, Water Resour. Res. 27, 1937–1945.
Markovich, K.H., Condon, L.E., Carroll, K.C., Purtschert, R., McIntosh, J.C., 2021. A mountain-front recharge component characterization approach combining groundwater age distributions, noble gas thermometry, and fluid and energy transport modeling. Water Resour. Res. 57. e2020WR027743.
Martel, D.J., O'Nions, R.K., Hilton, D.R., Oxburgh, E.R., 1990. The role of element distribution in production and release of radiogenic helium: the Carnmenellis Granite, southwest England. Chem. Geol. 88, 207–221.
Michalski, J.R., Onstott, T.C., Mojzsis, S.J., Mustard, J., Chan, Q.H.S., Niles, P.B., Johnson, S.S., 2018. The Martian subsurface as a potential window into the origin of life. Nat. Geosci. 11, 21–26.
Morrison, P., Pine, J., 1955. Radiogenic origin of the helium isotopes in rock. Ann. N.Y Acad. Sci. 62, 72–92.
Moser, H., Wolf, M., Fritz, P., Fontes, J.C., Florkowski, T., Payne, B.R., 1989. Deuterium, oxygen-18, and tritium in Stripa groundwater. Geochim. Cosmochim. Acta 53, 1757–1763.
Murseli, S., Middlestead, P., St-Jean, G., Zhao, X., Jean, C., Crann, C.A., Kieser, W.E., Clark, I.D., 2019. The Preparation of Water (DIC, DOC) and Gas (CO_2, CH_4) Samples for Radiocarbon Analysis at AEL-AMS, Ottawa, Canada. Radiocarbon 61, 1563–1571.
Musy, S., Casolaro, P., Dellepiane, G., Berger, A., Braccini, S., Purtschert, R., 2022. Quantification of ^{37}Ar emanation fractions from irradiated natural rock samples and field applications. J. Environ. Radioact. 251–252, 106966.
Neretnieks, I., 2013. Some aspects of release and transport of gases in deep granitic rocks: possible implications for nuclear waste repositories. Hydrogeol. J. 21, 1701–1716.
Nordstrom, D.K., Ball, J.W., Donahoe, R.J., Whittemore, D., 1989. Groundwater chemistry and water-rock interactions at Stripa. Geochim. Cosmochim. Acta 53, 1727–1740.
Nwaila, G., Frimmel, H.E., Minter, W.E.L., 2017. Provenance and geochemical variations in shales of the mesoarchean witwatersrand supergroup. J. Geol. 125, 399–422.
Onstott, T.C., Lin, L.-H., Davidson, M., Mislowack, B., Borcsik, M., Hall, J., Slater, G., Ward, J., Sherwood Lollar, B., Lippmann-Pipke, J., Boice, E., Pratt, L.M., Pfiffner, S., Moser, D., Gihring, T., Kieft, T.L., Phelps, T.J., Vanheerden, E., Litthaur, D., Deflaun, M., Rothmel, R., Wanger, G., Southam, G., 2006a. The Origin and Age of Biogeochemical Trends in Deep Fracture Water of the Witwatersrand Basin, South Africa. Geomicrobiol. J. 23, 369–414.
Onstott, T.C., McGown, D., Kessler, J., Sherwood Lollar, B., Lehmann, K.K., Clifford, S. M., 2006b. Martian CH_4: sources, flux, and detection. Astrobiology 6, 377–395.
Ozima, M., Podosek, F.A., 2002. Noble Gas Geochemistry. Cambridge University Press, Cambridge.
Parker, R.L., 1967. U.S. Geol. Survey Prof. Paper 440-D: Composition of the Earth's crust. In: Fleischer, M. (Ed.), Data of Geochemistry. first ed. United States Government Printing Office, Washington DC.
Phillips, F., Bentley, H., Davis, S., Elmore, D., Swanick, G., 1986. Chlorine 36 dating of very old groundwater: 2. Milk River Aquifer, Alberta, Canada. Water Resour. Res. 22, 2003–2016.
Phillips, F.M., Castro, M.C., 2003. 5.15 - Groundwater Dating and Residence-time Measurements. In: Holland, H.D., Turekian, K.K. (Eds.), Treatise on Geochemistry. first ed. Pergamon, Oxford, pp. 451–497.
Purtschert, R., Yokochi, R., Jiang, W., Lu, Z.T., Mueller, P., Zappala, J., Van Heerden, E., Cason, E., Lau, M., Kieft, T.L., Gerber, C., Brennwald, M.S., Onstott, T.C., 2021. Underground production of ^{81}Kr detected in subsurface fluids. Geochim. Cosmochim. Acta 295, 65–79.
Rueedi, J., Brennwald, M.S., Purtschert, R., Beyerle, U., Hofer, M., Kipfer, R., 2005. Estimating amount and spatial distribution of groundwater recharge in the lullemmeden basin (Niger) based on ^{3}H, ^{3}He and CFC-11 measurements. Hydrol. Process. 19, 3285–3298.
Sauvage, J.F., Flinders, A., Spivack, A.J., Pockalny, R., Dunlea, A.G., Anderson, C.H., Smith, D.C., Murray, R.W., D'Hondt, S., 2021. The contribution of water radiolysis to marine sedimentary life. Nat. Commun. 12, 1297.
Schlosser, P., Stute, M., Dörr, H., Sonntag, C., Münnich, K.O., 1988. Tritium/^{3}He dating of shallow groundwater. Earth Planet. Sci. Lett. 89, 353–362.
Sherwood Lollar, B., Westgate, T.D., Ward, J.A., Slater, G.F., Lacrampe-Couloume, G., 2002. Abiogenic formation of alkanes in the Earth's crust as a minor source for global hydrocarbon reservoirs. Nature 416, 522–524.
Sherwood Lollar, B., Onstott, T.C., Lacrampe-Couloume, G., Ballentine, C.J., 2014. The contribution of the Precambrian continental lithosphere to global H_2 production. Nature 516, 379–382.
Sherwood Lollar, B., Heuer, V.B., McDermott, J., Tille, S., Warr, O., Moran, J.J., Telling, J., Hinrichs, K.-U., 2021. A window into the abiotic carbon cycle – Acetate and formate in fracture waters in 2.7 billion year-old host rocks of the Canadian Shield. Geochim. Cosmochim. Acta 294, 295–314.
Silver, B.J., Raymond, R., Sigman, D.M., Prokopeko, M., Sherwood Lollar, B., Lacrampe-Couloume, G., Fogel, M.L., Pratt, L.M., Lefticariu, L., Onstott, T.C., 2012. The origin of NO_3 and N_2 in deep subsurface fracture water of South Africa. Chem. Geol. 294–295, 51–62.
Simkus, D.N., Slater, G.F., Sherwood Lollar, B., Wilkie, K., Kieft, T.L., Magnabosco, C., Lau, M.C.Y., Pullin, M.J., Hendrickson, S.B., Wommack, K.E., Sakowski, E.G., van

Heerden, Kuloyo, O., Linage, B., Borgonie, G., Onstott, T.C., 1980. Variations in microbial carbon sources and cycling in the deep continental subsurface. Geochim. Cosmochim. Acta 173, 264–283.
Slater, G.F., Lippmann-Pipke, J., Moser, D.P., Reddy, C.M., Onstott, T.C., Lacrampe-Couloume, G., Sherwood Lollar, B., 2007. 1^4C in Methane and DIC in the Deep Terrestrial Subsurface: Implications for Microbial Methanogenesis. Geomicrobiol. J. 23, 453–462.
Šrámek, O., Stevens, L., McDonough, W.F., Mukhopadhyay, S., Peterson, R.J., 2017. Subterranean production of neutrons, ^{39}Ar and ^{21}Ne: Rates and uncertainties. Geochim. Cosmochim. Acta 196, 370–387.
Sturchio, N.C., Du, X., Purtschert, R., Lehmann, B.E., Sultan, M., Patterson, L.J., Lu, Z.-T., Müller, P., Bigler, T., Bailey, K., O'Connor, T.P., Young, L., Lorenzo, R., Becker, R., El Alfy, Z., El Kaliouby, B., Dawood, Y., Abdallah, A.M.A., 2004. One million year old groundwater in the Sahara revealed by krypton-81 and chlorine-36. Geophys. Res. Lett. 31, L05503.
Sturchio, N.C., Kuhlman, K.L., Yokochi, R., Probst, P.C., Jiang, W., Lu, Z.-T., Mueller, P., Yang, G.-M., 2014. Krypton-81 in groundwater of the Culebra Dolomite near the Waste Isolation Pilot Plant, New Mexico. J. Contam. Hydrol. 160, 12–20.
Sudicky, E.A., Frind, E.O., 1981. Carbon 14 dating of groundwater in confined aquifers: Implications of aquitard diffusion. Water Resour. Res. 17, 1060–1064.
Tarnas, J.D., Mustard, J.F., Sherwood Lollar, B., Stamenković, V., Cannon, K.M., Lorand, J.-P., Onstott, T.C., Michalski, J.R., Warr, O., Palumbo, A.M., Plesa, A.-C., 2021. Earth-like habitable environments in the subsurface of mars. Astrobiology 21, 7.
Torgersen, T., Habermehl, M., Phillips, F., Elmore, D., Kubik, P., Jones, G., Hemmick, T., Gove, H., 1991. Chlorine 36 Dating of Very Old Groundwater: 3. Further Studies in the Great Artesian Basin, Australia. Water Resour. Res. 27, 3201–3213.
Tsang, C.F., Neretnieks, I., Tsang, Y., 2015. Hydrologic issues associated with nuclear waste repositories. Water Resour. Res. 51, 6923–6972.
Vinson, D.S., Tagma, T., Bouchaou, L., Dwyer, G.S., Warner, N.R., Vengosh, A., 2013. Occurrence and mobilization of radium in fresh to saline coastal groundwater inferred from geochemical and isotopic tracers (Sr, S, O, H, Ra, Rn). Appl. Geochem. 38, 161–175.
Visser, A., Fourré, E., Barbecot, F., Aquilina, L., Labasque, T., Vergnaud, V., Esser, B.K., 2014. Intercomparison of tritium and noble gases analyses, $^3H/^3He$ ages and derived parameters excess air and recharge temperature. Appl. Geochem. 50, 130–141.
Wang, K., Close, H.G., Tuller-Ross, B., Chen, H., 2020. Global average potassium isotope composition of modern seawater. ACS Earth Space Chem. 4, 1010–1017.
Warr, O., Sherwood Lollar, B., Fellowes, J., Sutcliffe, C.N., McDermott, J.M., Holland, G., Mabry, J.C., Ballentine, C.J., 2018. Tracing ancient hydrogeological fracture network age and compartmentalisation using noble gases. Geochim. Cosmochim. Acta 222, 340–362.
Warr, O., Giunta, T., Ballentine, C.J., Sherwood Lollar, B., 2019. Mechanisms and rates of ^4He, ^{40}Ar, and H_2 production and accumulation in fracture fluids in Precambrian Shield environments. Chem. Geol. 530, 119322.
Warr, O., Giunta, T., Onstott, T.C., Kieft, T.L., Harris, R.L., Nisson, D.M., Sherwood Lollar, B., 2021. The role of low-temperature ^{18}O exchange in the isotopic evolution of deep subsurface fluids. Chem. Geol. 561, 120027.
Warr, O., Ballentine, C.J., Onstott, T.C., Nisson, D.M., Kieft, T.L., Hillegonds, D.J., Sherwood, L.B., 2022. ^{86}Kr excess and other noble gases identify a billion-year-old radiogenically-enriched groundwater system. Nat. Commun. 13, 3768.
Warr, O., Song, M., Sherwood Lollar, B., 2023. The application of Monte Carlo modelling to quantify in situ hydrogen and associated element production in the deep subsurface. Front. Earth Sci. 11, 1150740.
Wassenaar, L., Aravena, R., Hendry, J., Fritz, P., 1991. Radiocarbon in dissolved organic carbon, A possible groundwater dating method: case studies from Western Canada. Water Resour Res. 27, 1975–1986.
Wigley, T.M.L., Plummer, L.N., Pearson, F.J., 1978. Mass transfer and carbon isotope evolution in natural water systems. Geochim. Cosmochim. Acta 42, 1117–1139.
Yang, I.C., Rattray, G.W., Yu, P., 1996. Interpretation of chemical and isotopic data from boreholes in the unsaturated zone at Yucca Mountain, Nevada. Water Resources Investigations Report. USGS Numbered Series 96-4058. U.S. Geological Survey, Denver.
Yizhao, C., Jianyang, X., Zhengguo, S., Jianlong, L., Yiqi, L., Chengcheng, G., Zhaoqi, W., 2015. The role of residence time in diagnostic models of global carbon storage capacity: model decomposition based on a traceable scheme. Sci. Rep. 5, 16155.
Yokochi, R., Sturchio, N.C., Purtschert, R., 2012. Determination of crustal fluid residence times using nucleogenic ^{39}Ar. Geochim. Cosmochim. Acta 88, 19–26.
Yokochi, R., Ram, R., Zappala, J.C., Jiang, W., Adar, E., Bernier, R., Burg, A., Dayan, U., Lu, Z.-T., Mueller, P., Purtschert, R., Yechieli, Y., 2019. Radiokrypton unveils dual moisture sources of a deep desert aquifer. Proc. Natl. Acad. Sci. 116, 16222–16227.
Zhou, Z., Ballentine, C.J., 2006. ^4He dating of groundwater associated with hydrocarbon reservoirs. Chem. Geol. 226, 309–327.
Zito, R., Donahue, D.J., Davis, S.N., Bentley, H.W., Fritz, P., 1980. Possible subsurface production of carbon-14. Geophys. Res. Lett. 7, 235–238.
Zivar, D., Kumar, S., Foroozesh, J., 2021. Underground hydrogen storage: A comprehensive review. Int. J. Hydrogen Energy 46, 23436–23462.